Graduate School ETD Form 9
(Revised 12/07)

PURDUE UNIVERSITY
GRADUATE SCHOOL
Thesis/Dissertation Acceptance

This is to certify that the thesis/dissertation prepared

By Matthew Ragozzino

Entitled
Multiresolution Variance-Based Image Fusion

For the degree of Master of Science in Electrical and Computer Engineering

Is approved by the final examining committee:

Paul Salama
Chair

Lauren Christopher

Maher Rizkalla

To the best of my knowledge and as understood by the student in the *Research Integrity and Copyright Disclaimer (Graduate School Form 20)*, this thesis/dissertation adheres to the provisions of Purdue University's "Policy on Integrity in Research" and the use of copyrighted material.

Approved by Major Professor(s): Paul Salama

Approved by: Brian King 4/23/2013
Head of the Graduate Program Date

MULTIRESOLUTION VARIANCE-BASED IMAGE FUSION

A Thesis

Submitted to the Faculty

of

Purdue University

by

Matthew Ragozzino

In Partial Fulfillment of the

Requirements for the Degree

of

Master of Science in Electrical and Computer Engineering

May 2013

Purdue University

Indianapolis, Indiana

To my family

ACKNOWLEDGMENTS

There have been many people who have inspired and encouraged me throughout my life, and without them, I would not be where I am now. To express my gratitude and thanks in words is a monumental task. This is my feeble attempt to thank those who have been there for me.

First of all, I would like to thank my parents, Joe and Linda. Without them to inspire and encourage me in my hopes and dreams, I cannot honestly say where I would be. To the rest of my family, I would like to thank you for your unending support and assistance, especially my sister Emily and my wonderful fiancé Ashley for their help in revising this thesis.

Special thanks to my adviser Dr. Paul Salama. I appreciate the guidance and the time that you took out of your busy schedule to advise me. It has been a pleasure working with you.

I would like to express my gratitude to the rest of my advisory board: Dr. Lauren Christopher and Dr. Maher Rizkalla. Thank you for all advising me throughout my time as a graduate student. I am eternally grateful.

Additionally, I would like to thank the entire administrative staff in the ECE department. Sherrie, Jeff, Jane, and Delana, you are the gears that keep the department moving.

Finally, I would like to thank NSCW Crane for contributing images.

TABLE OF CONTENTS

Page

LIST OF TABLES

LIST OF FIGURES

Figure Page

Figure Page

ABSTRACT

Ragozzino, Matthew. M.S.E.C.E., Purdue University, May 2013. Multiresolution Variance-Based Image Fusion. Major Professor: Paul Salama.

Multiresolution image fusion is an emerging area of research for use in military and commercial applications. While many methods for image fusion have been developed, improvements can still be made. In many cases, image fusion methods are tailored to specific applications and are limited as a result. In order to make improvements to general image fusion, novel methods have been developed based on the wavelet transform and empirical variance. One particular novelty is the use of directional filtering in conjunction with wavelet transforms. Instead of treating the vertical, horizontal, and diagonal sub-bands of a wavelet transform the same, each sub-band is handled independently by applying custom filter windows. Results of the new methods exhibit better performance across a wide range of images highlighting different situations.

1. INTRODUCTION

Image fusion has been a research topic dating back many decades, and the idea branches from a more generic research topic known as data fusion. According to [1], data fusion is classified as a framework that aims to provide methods and tools for the merger of data from different sources to improve the quality of information. The application of the methods and tools dictate the measure of quality and improvement of such.

Under the data fusion umbrella, image fusion is a broad topic itself. To precisely define the term, image fusion is the strategic combination of two or more images. Images can originate from both visible and infrared sensors or from the same sensor at different moments in time. Assuming two images meet the requirement of being properly registered, image fusion, according to [2], can produce images that are more suitable for human vision as well as computer vision for post-processing.

the general organization of this thesis will be given in 1.2.

1.1 Image Fusion Framework

Image fusion, in general, is a technique in which images from multiple sensors or multimodal imaging systems are merged together to create a new image with more information than any one of the constituent images [3]. Although any number of images can be fused together, practically tow or three are fused so as not to overwhelm an end user with the amount of information contained in the resulting image.

The fusion of images follows a general framework illustrated in Figure 1.1 below.

Image registration, which is the process of aligning images taken of the same object or scene at different times or through different sensors [4], is an essential aspect of

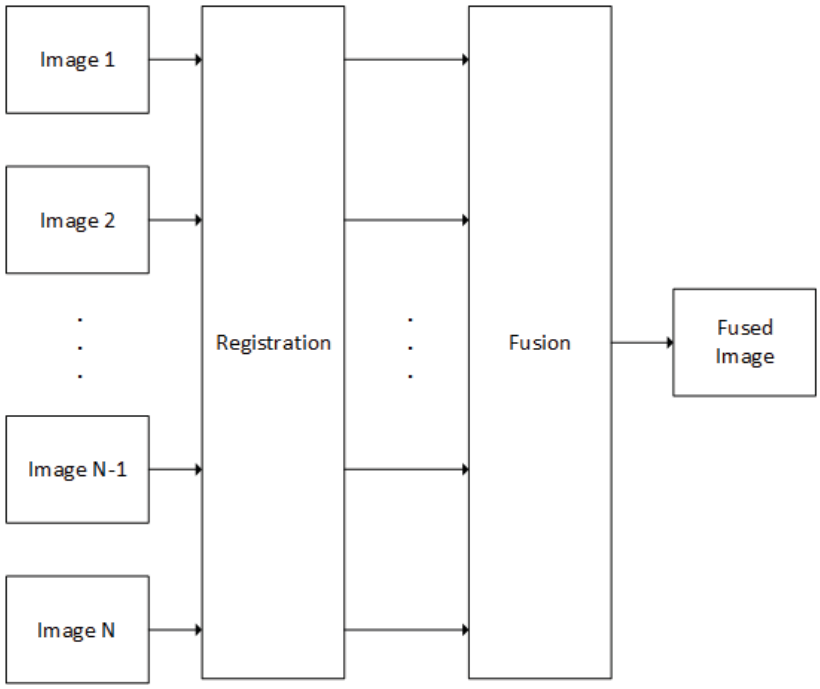

Fig. 1.1.: General framework for image fusion

image fusion. This is required to relate information in any two images [3]. Once image registration has been achieved, the process of fusing the input images begins.

There are many existing image fusion techniques. The most basic image fusion techniques include simple averaging the constituent images or selecting the greatest pixel value, while the more complex image fusion techniques include wavelet transforms or the IHS color transform to merge information.

In addition to different techniques implemented in the fusion stage, each technique can operate on one of the so called levels: "decision-level", "feature-level", and "pixel-level". Decision-level fusion is the highest level, feature-level is in the middle, and pixel-level is the lowest [5]. More details and examples of each level are presented in Chapter 2.

The target application also plays an important role in the fusion process. As mentioned above, there are many techniques, but some are developed for specific scenarios. Two areas of image fusion include multifocus image fusion and multisensor

image fusion. While multifocus and multisensor image fusion are not the only applications for image fusion, there is much research revolving around them, and methods that work for one application may not work for others.

Multifocus image fusion is one type of fusion that focuses primarily on images in the visible domain. When dealing with optical imaging systems, the ability to clearly identify objects is determined by a system's focal point. As the focal point changes, any object in front of or behind the focal plane will be out of focus [6]. Additionally, due to the fact that optical lenses suffer from a limited field of depth, an image where all objects appear sharp is impossible [6]. To overcome the limitations of optical lenses, multifocus image fusion has sought to combine the sharply focused regions of various images of the same scene [7].

Unlike multifocus image fusion, multisensor image fusion is not bound to optical imaging systems. As the name suggests, two or more sensors are used in multisensor image fusion. Because a single sensor can only operate in a specific range in the electromagnetic spectrum, multiple sensors can extend the viewing of a specific scene [8]. For example, the use of multisensor image fusion can help identify security breaches more effectively by merging visible and infrared images to account for changes in visible light. Image fusion is also used in conjunction with medical imaging. The ability to combine CT and MRI images can help doctors imporve diagnostic accuracy.

The military also has critical need for image fusion methods. Providing efficient fusion algorithms can assist in areas like target recognition. Just as with the commercial market, military security may also benefit from new and innovative fusion methods.

Throughout this thesis, the goal is to present novel fusion techniques that may be used in various applications. The focus will fall upon multiresolution image fusion; however, the methods presented may apply or provide insight to other fusion techniques like multifocus image fusion.

1.2 Thesis Organization

This thesis is organized as follows: In Chapter 2, a review of methods developed in the field of image fusion will be presented. Following, Chapter 3 will provide details about the methods developed, and Chapter 4 will present the results of each proposed method. Chapter 5 will conclude and provide suggestions for future work.

2. REVIEW OF LITERATURE

Throughout this chapter, a discussion of existing methods in the field of image fusion will be presented and discussed. The organization of the chapter will follow image fusion from the highest level to the lowest level (See Section 1.1 for details about the various levels of image fusion). In Section 2.1, a presentation of "decision-level" methods will take place followed by "feature-level" methods in Section 2.2, and finally a series of "pixel-level" methods will be discussed in Section 2.3 through Section 2.5. After presenting various techniques at each level, a high-level analysis of the methods will be provided in Section 2.6.

2.1 Decision-Level Methods

Decision-level fusion is considered to be the highest level of fusion [6]. Decision-level fusion methods fall into one of two categories: multimodal fusion or recognition. However, regardless of the category, each method follows a similar framework that fits within the fusion framework of Figure 1.1. In general, in decision-level image fusion, images are preprocessed, features are extracted and subsequently classified, and decisions are made based on the classification [9]. A general overview for decision-level fusion can be seen in Figure 2.1.

While both have the same framework, the outputs are different. The recognition methods produce an object identification from a predefined dictionary of responses. In the case of the latter, feature extraction and classification are performed and if enough of the classifiers agree, an identification is produced.

The first method for discussion is presented in [10] as a panchromatic sharpening (pansharpening) method for multiresolution remote sensing images. This method seeks to provide a new method for sharpening panchromatic satellite images by decid-

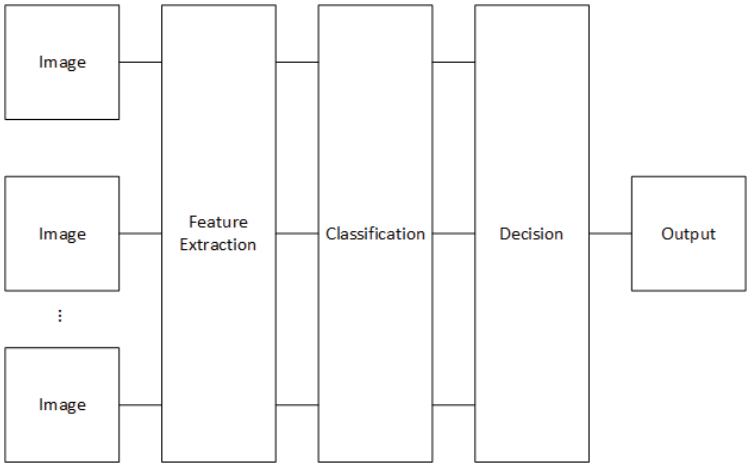

Fig. 2.1.: Framework for decision-level image fusion methods

ing between two existing pansharpening algorithms: À trous wavelet pansharpening (AWLP) and À trous wavelet transform followed by context-based decision fusion (AWCBD) [10]. Of course, this method can be classified as a multimodal fusion approach. While AWLP and AWCBD are not decision-level fusion techniques, the use of the two algorithms in tandem after classification makes the method in [10] a decision-level image fusion method.

Furthermore this method follows the framework defined in Figure 2.1 very closely. The method accepts two images, one image has a high spatial resolution and low spectral resolution, this is the panchromatic image. The other image has low spatial resolution and high spectral resolution, as is referred to as the visible image. The visible image is segmented into regions in the feature extraction stage, and once segmented, each region is classified as a small region or a large region. A decision is made between the two algorithms based on the region size classification. For each small region, the AWLP is applied while AWCBD is applied if the region is considered large.

Another set of methods that operate at the decision-level are presented in [9]. The methods presented are meant to be used for target recognition, thus each falls

in the recognition category of decision-level fusion. Unlike the algorithm presented in [10], these methods aim to classify what is in the image from a set of predefined choices. Using synthetic aperture radar (SAR) images, [9] attempts to recognize a target by classifying each image using a set of feature extraction algorithms and combine the results of each to make a decision. Principal Component Analysis (PCA), Linear Discriminate Analysis (LDA), and Independent Component Analysis (ICA) are utilized for feature extraction. In addition, there are three methods presented and analyzed in [9]: multi-view decision fusion, multi-feature decision fusion, and multi-classifier decision fusion.

In the multi-view decision fusion method, aerial images are taken of a target at different angles. Each angle is preprocessed and one of the mentioned feature extraction algorithms is applied. Once all the features are extracted, a single classifier is applied to each image, and the output of the classification stage is analyzed such that makes a decision on the target type is made.

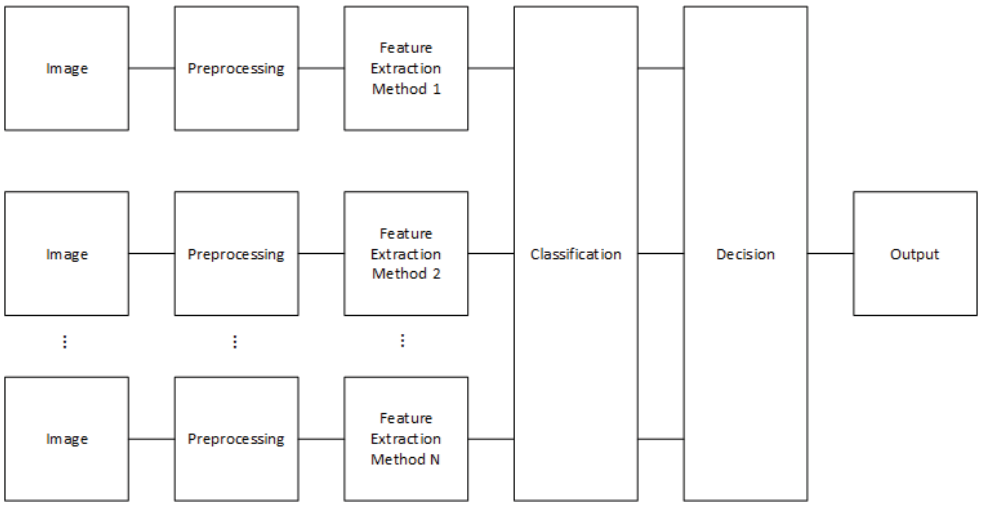

Fig. 2.2.: Multi-view decision method structure

The multi-feature decision fusion method is similar to the multi-view. Instead of multiple images taken at different angles, a single image is taken, preprocessed, and two or more feature extraction algorithms PCA, LDA, and ICA are applied [9]. The

same classifier is applied to the output of each feature extraction algorithm, and the output of the classification stage is sent to a decision process to identify the target.

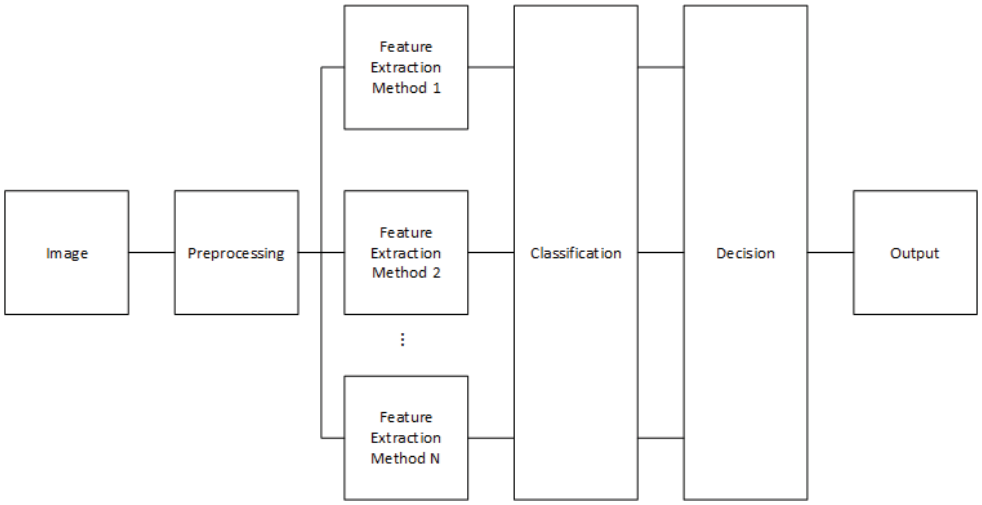

Fig. 2.3.: Multi-feature decision method structure

Finally, the multi-classifier decision fusion method has one image that is preprocessed and analyzed by one of the feature extraction algorithm: PCA, LDA, and ICA [9]. The output of the feature extractor algorithm is then sent to multiple classifiers and their outputs are sent to a decision process just like the multi-view and multi-feature decision methods.

The last method to be discussed that works at the decision-level is presented in [11]. Similar to [10], the proposed method in [11] applies to remote sensing images. The main difference, however, is that the scheme in [11] seeks to classify the regions of an image for remote sensing whereas [10] is concerned with improving the quality of the image. In terms of classification, this method would fall into recognition because it attempts to identify regions within an image using multiple classifiers. While recognition is the main focus of this method, the output is a not a single response from a predefined list as in [9]. The output is instead an image that is color coded to reflect the classification of each region.

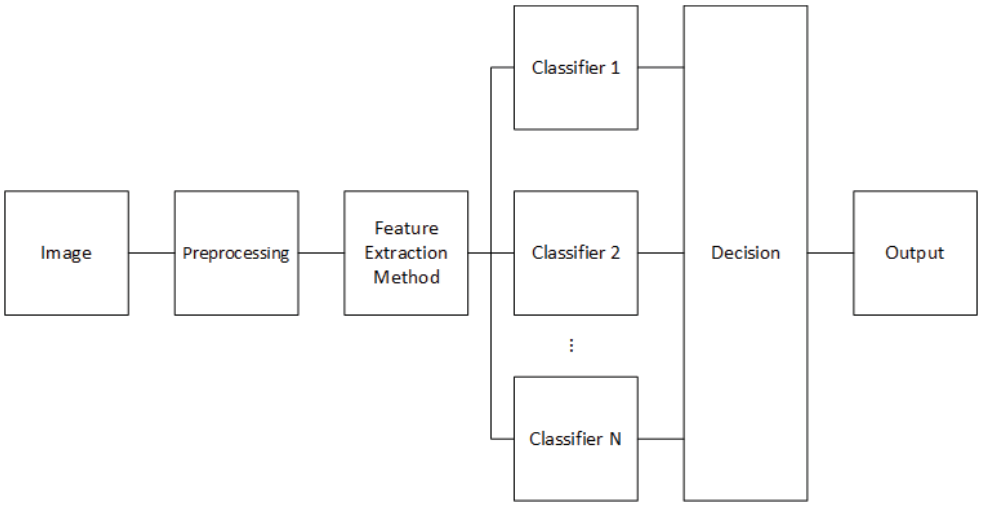

Fig. 2.4.: Multi-classifier decision method structure

In this method, a single image is processed, and after preprocessing, the image's features are extracted. Once the features are obtained, two or more sets of classifiers are applied to identify the various regions within the image. A decision is made between the set of classifiers, and the corresponding region in the output image is color coded to reflect the decision made. This method can be identified as a multi-classifier decision method as shown in Figure 2.4.

In decision-level image fusion, the main idea is to use multiple images to classify information. For some methods, like those found in [10], the goal is to take advantage of multiple methods to fuse information. Others, like the methods in [9] and [11], seek to identify information within images using a variety of feature extraction techniques and classification methods. In the following section, the next level of fusion, feature-level fusion, will be discussed. Unlike decision-level fusion, feature-level fusion does not aim to classify images or regions but uses features to segment regions within an image and fuse each region independently.

2.2 Feature-Level Methods

As previously mentioned, feature-level image fusion methods attempt to extract regions in the spatial domain to treat regions independently. The framework for feature-level image fusion is very similar to decision-level image fusion but excludes the classification stage. An overview for the feature-level image fusion process can be seen in Figure 2.5.

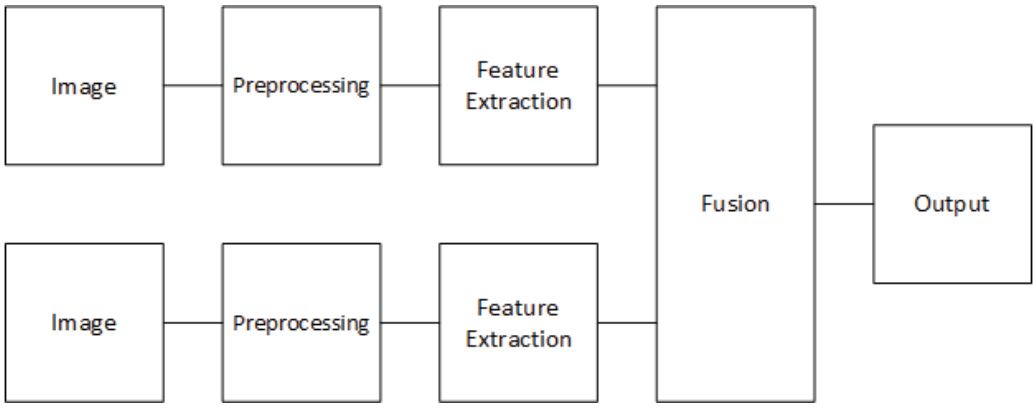

Fig. 2.5.: Framework for feature-level image fusion methods

Similar to decision-level fusion, the first two steps involve image preprocessing followed by feature extraction, although preprocessing is optional. Instead of classifying each region, the output of the feature extraction stage is sent to a fusion process where the regions calculated from the feature extraction process are fused.

In [12], a feature-level method is presented for multifocus image fusion. Multifocus image fusion methods accept two visible images taken at two different focal settings and attempt to consolidate the in-focus regions of each input image into a single image. In order to combine the in-focus regions of two input images into a single image, the method in [12] uses variance, gradients, and features of the input images in a series of steps. First, using generic properties of the input images, an optimal block size is calculated, and the input images are separated into the optimal block sizes. For each block, various features are extracted, and using a neural network, the

"clearness" is calculated. The clearness factor is used to decide which block will be used in the output image.

Another method, described in [13], is a feature-level image fusion algorithm that focuses on multisensor image fusion. In the proposed method, there are three main steps to fusing the input images. To start, an over-complete dictionary is created using the K-SVD algorithm which is a generalization of K-means clustering using singular value decomposition. In the next step, features are extracted and grouped the features using the dictionary in the first step into two categories: common components and innovation components. With the common and innovation components separated, fusion weights can be assigned independently. Common components will be fused with a low weight while innovation components will be assigned a weight based on the level of activity within the source image.

Similar to [13], the method presented in [14] focuses on multisensor image fusion. However, unlike [13], the method presented in [14] utilizes segmentation and wavelet transforms to fuse images. Initially, images are decomposed using wavelet transforms. Based on the output of the wavelet transforms, the input images are segmented using algorithms developed in [15, 16]. Once the segmentation stage, also known as the feature extraction stage is complete, the segmented regions are sent on to the fusion process.

The fusion process presented in [14] is applied to each region output from the segmentation stage. Utilizing bitvariate alpha-stable distributions, the important regions are identified in the original images. From the important information, a mapping is generated from the coefficients produced by the bitvariate alpha-stable distribution. These coefficients are utilized as fusion weights.

Feature-level image fusion has some advantages over other levels of fusion by providing isolation of regions within an image; however, segmentation may be difficult if too much or too little information exists in the input images. In the next sections, various low level techniques, referred to as pixel-level techniques will be described.

The first technique will be IHS transforms followed by wavelet transforms. Finally, other various techniques will be presented.

2.3 IHS Transform Based Methods

The Intensity-Hue-Saturation (IHS) transform is a process for converting an image in the red, green, and blue (RGB) color space to the IHS color space. In order to utilize any IHS transform fusion methods, one of the input images must be represented in the RGB color space. The transformation from RGB to IHS used in [17] is

$$\begin{bmatrix} I \\ H \\ S \end{bmatrix} = \begin{bmatrix} \frac{1}{3} & \frac{1}{3} & \frac{1}{3} \\ \frac{-\sqrt{2}}{6} & \frac{-\sqrt{2}}{6} & \frac{2\sqrt{2}}{6} \\ \frac{1}{\sqrt{2}} & \frac{-1}{\sqrt{2}} & 0 \end{bmatrix} \begin{bmatrix} R \\ G \\ B \end{bmatrix}. \tag{2.1}$$

Like decision-level and feature-level methods, methods that utilize IHS transforms follow a generic framework given in Figure 2.6.

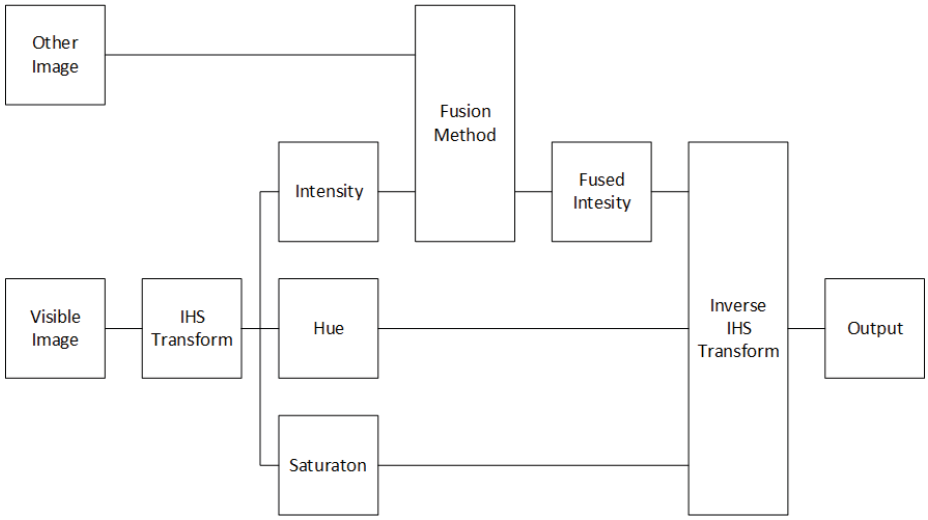

Fig. 2.6.: Framework for IHS transform image fusion methods

In all IHS transform based methods, an image in the RGB color space, usually a visible spectrum image, serves as one of the inputs. The other image can be an

infrared image or a high resolution image. Using Equation 2.1, the visible image is transformed, and the intensity component, $\boldsymbol{I}$, extracted. The intensity component and the other source image are fused together into a new intensity component, $\boldsymbol{I}_F$. $\boldsymbol{I}_F$ replaces $\boldsymbol{I}$, and the inverse IHS transform is performed to generate the fused image.

The first IHS based method for discussion was developed by [18] and focuses on remote sensing applications. In remote sensing image fusion there are typically two images: a panchromatic image which has high spatial resolution but low spectral resolution, and a visible image with low spatial resolution but high spectral resolution. The objective is to replace some information in the visible image, which is represented in the RGB color space, with the panchromatic image. The panchromatic image is represented as a grayscale image.

The method in [18] initially transforms the visible image from the RGB color space to the IHS color space using Equation 2.1. Once in the IHS color space, the intensity component is replaced with the panchromatic image. Finally, the image is transformed back to the RGB color space.

In addition to the simple fusion rule, [18] introduces a value t, where $t \in [1, \infty)$, that determines the weight between the panchromatic image and the visible image. When $t = 1$, the panchromatic image is not included in the fused image. As $t \to \infty$, the panchromatic image has more weight than the visible image.

Another method that uses IHS transforms for remote sensing applications is described in [19]. Again, the visible images have low spatial resolution in the RGB color space, while panchromatic images are represented as grayscale images. The main difference between the methods in [18] and [19] is how the weights between the intensity of the visible image and the panchromatic image are calculated. Instead of using a user-defined weight, [19] uses statistical features within the intensity of the visible image and the panchromatic image. The fused intensity is calculated using a regional expectation E_R. For each pixel (i, j), the expectation is obtained using a 3×3 window, represented as R, with (i, j) as the center. Denoting $\boldsymbol{I}_V$ as the intensity

of the visible image and $\boldsymbol{I}_P$ as the panchromatic image, then the fused intensity is $\boldsymbol{I}_F$ found using

$$\boldsymbol{I}_F(i,j) = E_R\{\boldsymbol{I}_V(i,j)\} + (\boldsymbol{I}_P(i,j) - E_R\{\boldsymbol{I}_P(i,j)\})\,. \tag{2.2}$$

Similar to [18], $\boldsymbol{I}_F$ replaces $\boldsymbol{I}_V$, and the inverse IHS transform is used to generate the fused image.

Another method that is similar to the previous two methods is proposed by [20]. The main goal of this method is to fuse multiple satellite images while enhancing vegetation information.

The proposed method in [20] is a six step process following the framework in Figure 2.6. First, the visible image is transformed to the IHS color space, and an index, known as HRNDVI, is calculated to determine the amount of vegetation within the original visible image. The new intensity component is obtained using the intensity from the visible image and the panchromatic image using a method similar to that presented in [18]. After the new intensity image is determined, the fused image is formed by reverting back to the RGB color space using the new intensity image. Finally, enhancements to the vegetation components are made by adding to the G and B components of the fused image using the HRNDVI to calculate the weight for each pixel.

The final method, which is unlike any of the first three methods, is presented in [21]. This method is mainly focused on multisensor image fusion, particularly infrared and visible image fusion. Even though the application for this particular method is for multisensor image fusion, the framework in Figure 2.6 is still followed.

In order to fuse visible and infrared images, [21] proposes the following method: first, transform the visible image represented in the RGB color space to the IHS color space. Decompose the infrared image and the intensity component of the visible image with the dual-tree complex wavelet transform. For each high pass image, fuse the information from the infrared and visible images using a covariance based method.

Next, average the low-pass images. Once the fused low and high pass images are processed, reconstruct a new intensity component using the inverse wavelet transform. Finally, utilize the inverse IHS transform to obtain the fused image.

As an image fusion technique, IHS transforms offer some advantages over other techniques. The main advantage is maintaining color in the fusion process; however, not all applications require or allow color throughout the fusion process. In the next section, wavelet transforms will be presented. Using wavelet transforms as a method for fusion provides a certain level of control that many methods lack. Additionally, wavelets can be adapted to almost any fusion situation.

2.4 Wavelet-Based Methods

In terms of image fusion, using wavelets is one of the most popular techniques. There are many applications of wavelets in multisensor, multifocus, and multiresolution image fusion. Using wavelets provides a way to isolate frequency content while maintaining time or, in the case of images, spatial characteristics [22]. Just as with other techniques, wavelet fusion methods follow a framework that can be seen in Figure 2.7.

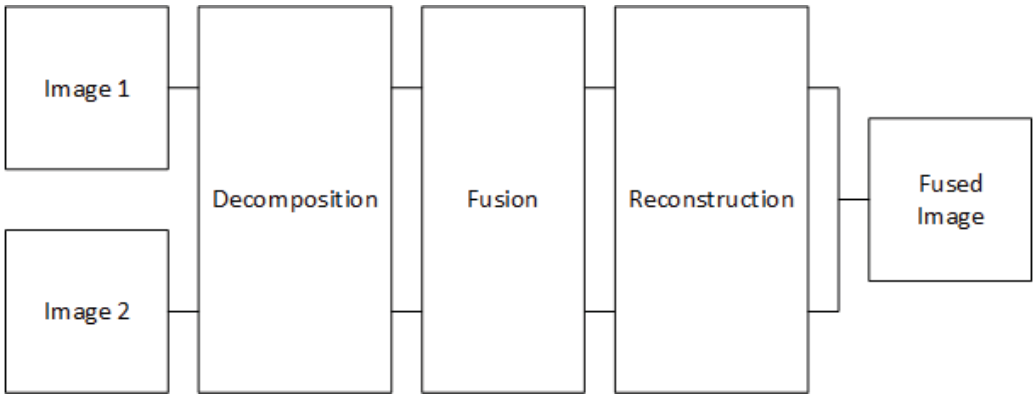

Fig. 2.7.: Framework for wavelet image fusion methods

All wavelet image fusion methods follow a basic three step process. First, images are decomposed using a wavelet transform. After decomposition, a fusion rule is applied to each subband image. Finally, the subbands that were generated in the fusion process are reconstructed.

Early in the development of wavelet-based image fusion methods, [23] presented three simple techniques for fusing panchromatic images and visible images for remote sensing applications. Like many remote sensing methods, there are usually two inputs: a low resolution image represented in the RGB color space, referred to as the visible image, and a high resolution grayscale image, referred to as the panchromatic image. All three techniques rely on wavelet transforms for fusion, particularly the À trous wavelet algorithm [23]. The first method is a substitution method, the second an additive method, and the third uses the IHS transform for fusion.

The first technique can be described as a simple substitution subsequent to the wavelet decomposition. After registration and preprocessing of the images, the visible and panchromatic images are decomposed using two or three levels of decomposition. Within the decomposed visible and panchromatic images, the high-pass subbands of the panchromatic image replace the high-pass subbands of the visible image. Once the image substitution is complete, the inverse wavelet transform is applied to the visible image to produce the output.

Next, [23] proposes an additive method for image fusion. The additive method is similar to the substitution method in that the panchromatic image is decomposed. However, the low resolution image is left as is. After extracting the R, G, and B components out of the low resolution image, the high frequency content of the panchromatic image is directly added to the R, G, and B components of the visible image. The new R, G, and B components are then combined to form the new, fused image.

The third and final method proposed by [23] is very similar to the second method. Instead of using the R, G, and B components of the visible image, they are IHS color space. The high-pass subband images of the panchromatic image are then added to

the intensity component of the visible image. Once the addition is complete, the image is reverted back to the RGB color space to form the newly fused image.

Another method developed for application in remote sensing is given in [24]. Instead of adding or substituting subband images, the proposed method uses variance to fuse images together. Again, in remote sensing applications, there are two images, a visible image and a panchromatic image. In order to fuse the images, each input image is decomposed via a wavelet transform. After the decomposition is complete, regional variance of each subband images is found. Regional variance of the coefficients neighboring (k, l) in each high-pass subband, defined as $\sigma_2(k, l)$, is obtained for the visible and panchromatic images as used in the following fusion rule: for each coefficient (k, l) in each high frequency subband image, the newly fused image $F(k, l)$ is constructed using the following:

$$F(k,l) = \begin{cases} V(k,l) & \text{if } \sigma_V^2(k,l) \geq \sigma_P^2(k,l) \\ P(k,l) & \text{if } \sigma_V^2(k,l) < \sigma_P^2(k,l) \end{cases} \tag{2.3}$$

where V is the visible image and P is the panchromatic image. As this rule is not applied ot the low frequency subband images, they are averaged together. Next, the inverse wavelet transform is applied to produce the final fused image.

Fusion of two images of the4 same scene taken with different focal settings is presented in [25]. Again, wavelets are used to perform the fusion, and similar to [24], the method uses statistics to fuse the information between the two images. In particular, two levels of decomposition are used to create one low-pass image and six high-pass images.

For each low-pass image, the energies are obtained in a window around each pixel (k, l). Using the energy between the two low-pass images, a weight is produced. The weight is then used to average the new low-pass images together.

Once the low-pass images are fused, the six high-pass images are fused using a different rule. The information in the high-pass images is fused using a covariance based rule instead of energy, as covariance is used to measure the dispersion in a

region around a coefficient (k, l) [25]. For a given region defined around a coefficient (k, l), if one image is in focus and the other out of focus, then the in-focus image will have more weight in the fused high-pass image. After applying the energy rule to the low-pass image and the covariance rule to the high-pass image, the inverse wavelet transform is applied to produce the new, fused image.

In [6], another method is presented that applies to multifocus image fusion using statistical properties like [25]. Instead of using covariance, the method uses regional variance. Again, the wavelet decomposition is applied to the input images, and a low-pass image and several high-pass images are created. The regional variance is then obtainted for both the low-pass and high-pass images. For the low-pass, a weighted average is applied to produce the fused low-pass image whereas for the the high-pass images, the regional variance is used to obtained the "sharpness" of an image at a given coefficient (k, l). The fused high-pass image, F, is created by a decision that is similar to Equation 4.4. After generating the fused low and high-pass images, the inverse wavelet transform creates the final fused image.

Another method that is similar to [25] and [6] is presented in [26]. Using statistical properties, information between two decomposed images is fused together. Unlike [25] and [6], [26] applies to medical images, specifically the fusion of a CT image and an MRI image. Additionally, the approach in [26] applies a simple rule to the high-pass image while using a covariance based rule on the low-pass image. After applying a wavelet decomposition to the two input images (two levels of decomposition are recommended), the covariance of the two low-pass images is used to generate a coefficient matrix with values between 0 and 1. The coefficient matrix is used to define the weighted average between the two low-pass images. As for the high-pass images, a simple maximum value selection method between two corresponding high-pass images is applied. The inverse wavelet transform is applied to produce the fused image.

Another method that utilizes statistical properties in fusion is presented in [3]. The proposed method focuses on removing noise and using the properties of wavelet

transforms to fuse multisensor and multimodal images. After removing noise from the input images, each input is decomposed using wavelet transforms. Using the standard deviation to measure contrast and signal-to-noise ratio, the subimages are fused together. For regions in the images that have a high signal-to-noise ratio, the weight of each image is proportional to the contrast. Otherwise, if the signal-to-noise ratio is low, the weight is inversely proportional to the contrast. The inverse wavelet transform is applied to generate the fused image.

In [5], four methods are proposed using the stationary wavelet transform. The first and second are both based on choosing maximum values. The first works at the pixel level while the second takes each decomposed subimage into account. The third method is similar to the second method but uses regional variance, and the four and final method is based on covariance.

As mentioned above, the first two methods are based on the principal of choosing the max between the two images to be fused. The first works at the pixel level. For each high-pass image after wavelet decomposition, the pixels are compared, and the pixel with the greatest magnitude is picked to be in the fused image. The second method is similar to the first, except instead of looking at each high-pass image independently, all the subimages are considered at the same time. At a given location, (k, l), the values are summed across the the high-pass subimages. The subimages with the highest sum are placed in the fused subimages. The inverse wavelet transform is applied to produce the final fused image.

The third method is based on variance and has a similar principal to the second method. Instead of focusing on a single subimage, each high-pass subimage is used to calculate the fused image. In the third method, regional variance is calculated in each subimage and summed across the three high-pass subimages. The max value is then used to choose between the two input images.

Finally, the fourth method uses a different approach by utilizing covariance between the two input images. Decisions are made on a pixel by pixel basis from the results of the covariance matrix for each high-pass subimage. If the covariance matrix

is below some threshold, the variance decides which image contributes to the fused image. Otherwise, the two subimages are fused using a weighed average based on the calculated covariance.

The last wavelet based method is proposed by [27]. The proposed method is unlike any other method discussed thus far. Most wavelet based method focus on a static number of decomposition stages whereas in [27], the number of decomposition levels varies based on a rule. Given a threshold which is a parameter of the method, a coefficient based on each entire subimage is calculated. If the coefficient is greater than the threshold, the subimage is decomposed and the threshold calculation is applied to each decomposed image. On the other hand, if the coefficient is less than the threshold, a fusion rule is applied. No particular rule is suggested in [27], but most rules discussed thus far may apply. The inverse wavelet transform is applied to each level until a single fused image is reached.

Wavelet transform based image fusion techniques provide a robustness that other methods lack. Using wavelets is by far the most popular technique in image fusion as they provide the ability to adapt to many scenarios and applications. While very popular, there are many methods other than the wavelet transform based method and some of these are presented in the next section.

2.5 Other Methods

In addition to the wavelet transform and IHS transform based methods, there are other methods that utilize Brovey Transforms, high-pass filtering, high-pass modulation, Principal Component Analysis (PCA), Hidden Markov Trees, and Genetic Algorithms.

A method that uses a pyramid fusion scheme coupled with PCA is presented in [28]. Once each input image is decomposed using a pyramid decomposition scheme, the k^{th} level is fused by using a 3×3 window to calculate the weights for fusion using

a PCA method. After the k^{th} level is fused, the $k^{th} - 1$ level is fused, and so on until the top level is reached.

In [29], a method is proposed to fuse visible and infrared images using a Hidden Markov Tree based decomposition approach. The method is similar to wavelet decomposition; however, the Hidden Markov Tree distributes coefficients to subimages differently. Once decomposition is complete and the energy around each pixel in the decomposed images is used for fusion, the fused image is constructed.

Three methods based on genetic algorithms are described in [30]. The first proposed method is a simple weighted average between two input images where genetic algorithms are used to identify the optimal weight between the two images.

In the second method, [30] suggest that the input images be transformed to the wavelet domain. Within the wavelet domain, on a pixel by pixel basis for each subband image, a genetic algorithm is used to decide weather the pixel from one image or the other is used in the fused image.

The final method proposed in [30] is a threshold selection algorithm. Since the proposed methods aim to work with multisensor data, thresholds are checked against the infrared image data. The innovation in this method occurs in genetic algorithms should be used to select the optimal threshold value [30]. If the infrared image data is greater than the threshold, the pixel from the infrared image is placed in the fused image, otherwise the visible image pixel is selected.

In the next section a qualitative analysis of the various levels and techniques of fusion will be conducted. The results of this analysis will provide reasoning for the decision to develop the methods that are presented in Chapter 3.

2.6 Qualitative Analysis

Throughout this chapter, a presentation of the different levels of image fusion have been presented. Decision, feature, and pixel image fusion levels have been described, and techniques for each level have been discussed. Throughout this section, each level

of fusion will be discussed and the conclusions will directly influence the approaches that will be presented in Chapter 3.

The first level of fusion discussed in this chapter was decision-level image fusion. Throughout the methods presented in Section 2.1, a recurring theme present was that decision-level image fusion seeks to classify and identify objects within a scene. In [9], decision-level fusion is regarded as an recognition tool.

While decision-level fusion is great for recognition, there are many negative aspects. First of all, the decision-level image fusion process is very selective. Typically, classification is predefined by a dictionary. Elements or regions of the input images are placed in one of the predefined categories. This leads to the second issue with decision-level fusion: improper identification. If an element or region in an image does not fit in one of the predefined categories, the element or region in question may be forced to associate to one of the predefined classifications. Lastly, preparation is a major step in decision-level fusion. In order to classify elements or regions within an image, training is usually a major step before the algorithm can be implemented.

Feature-level fusion, unlike decision-level fusion, does not seek to classify elements or regions within an image. Instead, feature-level fusion attempts to separate regions and elements so that each region can be handled independently in the fusion process. In [14], some of the benefits of feature-level image fusion include reduced sensitivity to noise, enhanced features, and smart selection of fusion rules due to the independence previously mentioned.

Even though isolation of regions within an image may assist in the image fusion, the feature extraction process is not always exact, especially when dealing with features from multiple sensors. For example, the features extracted from each sensor may not line up exactly as expected between an infrared and visible spectrum image. Furthermore, identifying regions between two images may be difficult, and if fusion techniques between adjacent regions are acting independently using different settings or different rules, distortion and misrepresentation of data may occur in the fused image.

When using IHS transforms for image fusion, there is a clear advantage over other methods: color information is preserved throughout the process of fusion. However, not all applications require that color information be preserved. Additionally, according to [20], the use of IHS transforms for image fusion may also introduce color distortion.

The most robust methods for image fusion use wavelet transforms. The distinct advantage of wavelet transforms over other techniques is the isolation of spectral information while maintaining time or spatial characteristics. Like the feature-level fusion techniques, wavelets isolate regions so that information in different spectral ranges can be handled independently. Unlike feature-level image fusion, however, wavelet spectral regions are predefined, and the process of wavelet decomposition can be implemented iteratively to refine the isolation of spectral regions.

While wavelet transforms are very popular and robust for image fusion, there are some negative aspects. The first negative aspect to using wavelet transforms applies to the process of decomposition and reconstruction. Discrete wavelet transforms are not shift-invariant [7]. Additionally, wavelet transforms are not dynamic. The filters are predefined, and in order to isolate specific frequencies, more levels of decomposition may be required.

Despite the limitations of wavelet transforms, their advantages outweigh the disadvantages. When the information in the input images is unknown, a robust method for fusion is needed. Using decision and feature-level image fusion techniques will not fulfill this requirement. While using IHS transforms may be robust when information is unknown, the applications in which IHS transform methods can be used is limited. Additionally, while there are many other techniques for image fusion, many are still underdeveloped or cannot compete with existing techniques. From the analysis of these various methods, a set of methods using wavelet transforms have been developed and presented in Chapter 3. Following the presentation of the developed methods, the results will be discussed in Chapter 4.

3. METHODS

Details about each method will presented in Sections 3.3 through 3.7. This chapter describes new fusion methods based on the wavelet transform and regional variance.

3.1 Wavelet Transforms

Wavelet-based image fusion methods follow a general framework. Decomposition, fusion, and reconstruction are the typical stages in wavelet-based image fusion methods (see Figure 2.7). Within this general structure, the major difference between methods is the fusion stage; the decomposition and reconstruction elements in each method are very similar.

Through out this section, the various stages within the framework of wavelet-based image fusion methods will be discussed. In Section 3.1.1, the decomposition stage will be presented in detail. Following decomposition, general fusion will be discussed in Section 3.1.2. Finally, reconstruction is presented in Section 3.1.3.

3.1.1 Decomposition

For one-dimensional discrete-time signals, a single-level wavelet decomposition takes a signal, $x[n]$, as an input and generates two signals: one that contains the low frequency content of $x[n]$ and the other which contains the high frequency content. These are denoted as $x_L[n]$ and $x_H[n]$ respectively. In order to create $x_L[n]$ and $x_H[n]$, the signal is first passed through two filters: a low-pass filter $h_1[n]$ and a high-pass filter $g_1[n]$. By passing $x[n]$ through $h_1[n]$ and $g_1[n]$, the signals $y'_L[n]$ and $y'_H[n]$ are generated, and $y_L[n]$ and $y_H[n]$ are produced by down-sampling $y'_L[n]$ and $y'_H[n]$ by a factor of 2. The one-dimensional process of decomposition can be seen in Figure 3.1.

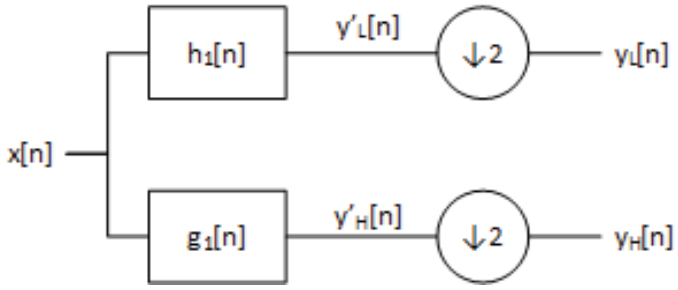

Fig. 3.1.: One-dimensional single-level wavelet decomposition overview

The decomposition process is not limited to a single level. In many cases, decomposition is applied multiple times and usually to the low pass signals to further isolate the frequencies of the original signal $x[n]$. A visual representation of multi-level decomposition is presented in Figure 3.2.

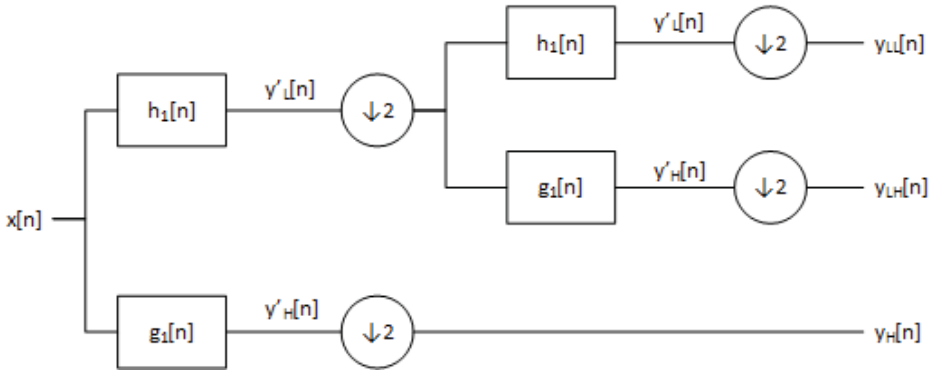

Fig. 3.2.: One-dimensional multi-level wavelet decomposition overview

Applying wavelet decomposition to two-dimensional signals is a simple process. Instead of a one-dimensional signal, the input to the wavelet decomposition process is an $N \times M$ array denoted as $\boldsymbol{X}$. The first step to decomposing a two-dimensional array is to perform a one-dimensional wavelet decomposition on each column. From this process two matrices are produced with approximately half the height of the $\boldsymbol{X}$ assuming $N >>$ length$(h[n])$ and length$(h[n])$ = length$(g[n])$. $\boldsymbol{X}_L$ and $\boldsymbol{X}_H$ will represent the new matrices. After the two matrices are created, each row of $\boldsymbol{X}_L$ and

$\boldsymbol{X}_H$ are decomposed using the same process that the columns used. The result will produce four matrices that are approximately half the size of the original matrix. The decomposed rows of $\boldsymbol{X}_L$ will produce $\boldsymbol{X}_{LL}$ and $\boldsymbol{X}_{LH}$, and the decomposed rows of $\boldsymbol{X}_H$ will produce $\boldsymbol{X}_{HL}$ and $\boldsymbol{X}_{HH}$ as shown in Figure 3.3.

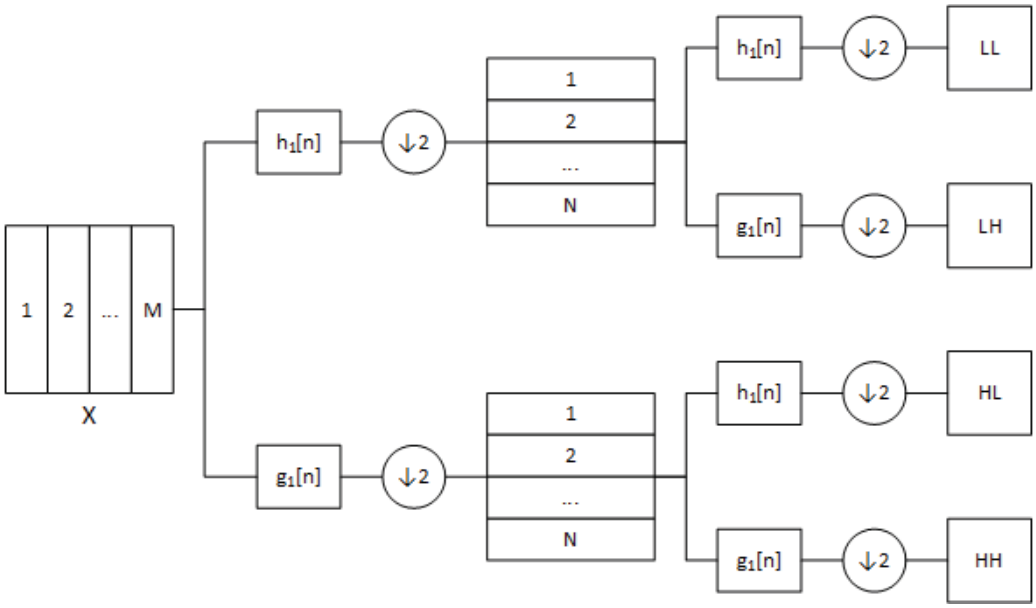

Fig. 3.3.: Two-dimensional single-level wavelet decomposition overview

3.1.2 Fusion

From the decomposition stage, two input images $\boldsymbol{X}$ and $\boldsymbol{Y}$ are each broken down into four smaller images. $\boldsymbol{X}_{LL}$, $\boldsymbol{X}_{LH}$, $\boldsymbol{X}_{HL}$, and $\boldsymbol{X}_{HH}$ are extracted from $\boldsymbol{X}$ and $\boldsymbol{Y}_{LL}$, $\boldsymbol{Y}_{LH}$, $\boldsymbol{Y}_{HL}$, and $\boldsymbol{Y}_{HH}$ from $\boldsymbol{Y}$. The images denoted by a subscript LL refer to the low-pass images. Subscripts LH, HL, and HH refer to high-pass images. In most cases, the low-pass image and the high-pass images are treated independently from one another.

For all cases, the fusion stage attempts to extract the most important elements from the input images and consolidate them into a single image. If the fused image is denoted by $\boldsymbol{Z}$, then the LL, LH, HL, and HH versions of $\boldsymbol{X}$ and $\boldsymbol{Y}$ are used

to created $\boldsymbol{Z}_{LL}$, $\boldsymbol{Z}_{LH}$, $\boldsymbol{Z}_{HL}$, and $\boldsymbol{Z}_{HH}$. After each image is fused, the decomposed images of $\boldsymbol{Z}$ are sent to the final stage: reconstruction.

3.1.3 Reconstruction

The final stage for wavelet based image fusion is the reconstruction stage, sometimes referred to as synthesis. Within this stage, the four images output from the fusion process, $\boldsymbol{Z}_{LL}$, $\boldsymbol{Z}_{LH}$, $\boldsymbol{Z}_{HL}$, and $\boldsymbol{Z}_{HH}$, are taken as inputs and merged to create the final output $\boldsymbol{Z}$.

For a pair of one-dimensional, discrete-time signals $y_L[n]$ and $y_H[n]$, reconstruction is achieved by reversing the decomposition process. $y_L[n]$ and $y_H[n]$ are first upsampled by a factor of 2, filtered by $h_2[n]$ and $g_2[n]$ to produce $x_L[n]$ and $x_H[n]$ respectively. Reconstruction is completed by summing $x_L[n]$ and $x_H[n]$ to produce $\hat{x}[n]$. A visual representation of the reconstruction process can be seen in Figure 3.4.

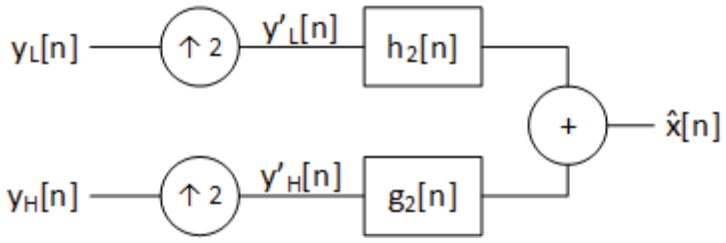

Fig. 3.4.: One-dimensional single-level wavelet reconstruction overview

As mentioned in Section 3.1.1, the process of decomposition can be applied multiple times. For each level a signal is decomposed, reconstruction needs to be applied. For example, if a signal $x[n]$ is decomposed twice, then reconstruction will be applied twice. In order to reconstruct two or more levels, the reconstruction stage is cascaded together. See Figure 3.5 for more details.

Similar to the two-dimensional decomposition process, two-dimensional reconstruction processes the rows and columns separately. With four arrays, $\boldsymbol{Z}_{LL}$, $\boldsymbol{Z}_{LH}$,

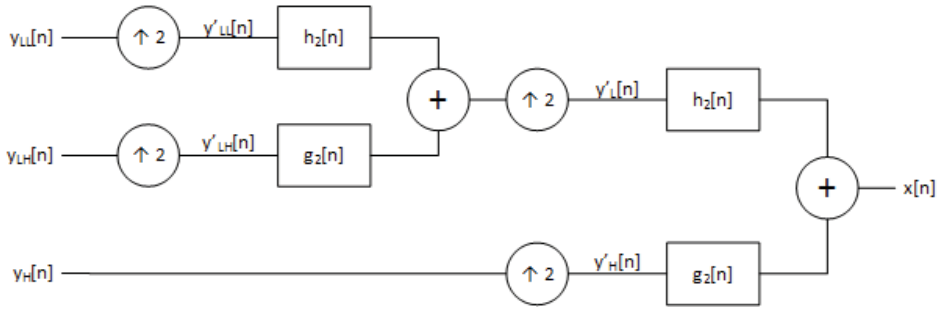

Fig. 3.5.: One-dimensional multi-level wavelet reconstruction overview

$\boldsymbol{Z}_{HL}$, and $\boldsymbol{Z}_{HH}$, as inputs, $\boldsymbol{Z}_{LL}$ and $\boldsymbol{Z}_{LH}$ are grouped together, and $\boldsymbol{Z}_{HL}$ and $\boldsymbol{Z}_{HH}$ are grouped together. The rows are processed first. Looking at the first group comprised of $\boldsymbol{Z}_{LL}$ and $\boldsymbol{Z}_{LH}$, each row of the two images is processed by the one-dimensional reconstruction process highlighted in Figure 3.4. The resulting array will be $\boldsymbol{Z}_L$. Duplicating the process for the group containing $\boldsymbol{Z}_{HL}$ and $\boldsymbol{Z}_{HH}$, the array $\boldsymbol{Z}_H$ is created. Using $\boldsymbol{Z}_L$ and $\boldsymbol{Z}_H$ as inputs, each column is processed by the one-dimensional reconstruction process to produce $\boldsymbol{Z}$. Details for the process can be seen in Figure 3.6.

Throughout the processes of decomposition and reconstruction, four filters are mentioned, $h_1[n]$, $g_1[n]$, $h_2[n]$, and $g_2[n]$. Filters in the decomposition and reconstruction stages are not arbitrarily assigned; instead, each filter is carefully chosen to achieve perfect reconstruction [22].

In terms of image fusion, there are several sets of wavelet filters that are used. Orthogonal and Bi-orthogonal wavelet filters are the most common wavelet filters used in image fusion. In [31], a study was conducted to compare the efficiency of the various filters within the Orthogonal and Bi-orthogonal wavelet families. As a result of the study, a Bi-orthogonal wavelet filter was suggested for image fusion. Throughout each method, a Bi-orthogonal wavelet filter was used to decompose the input images and reconstruct the fused image.

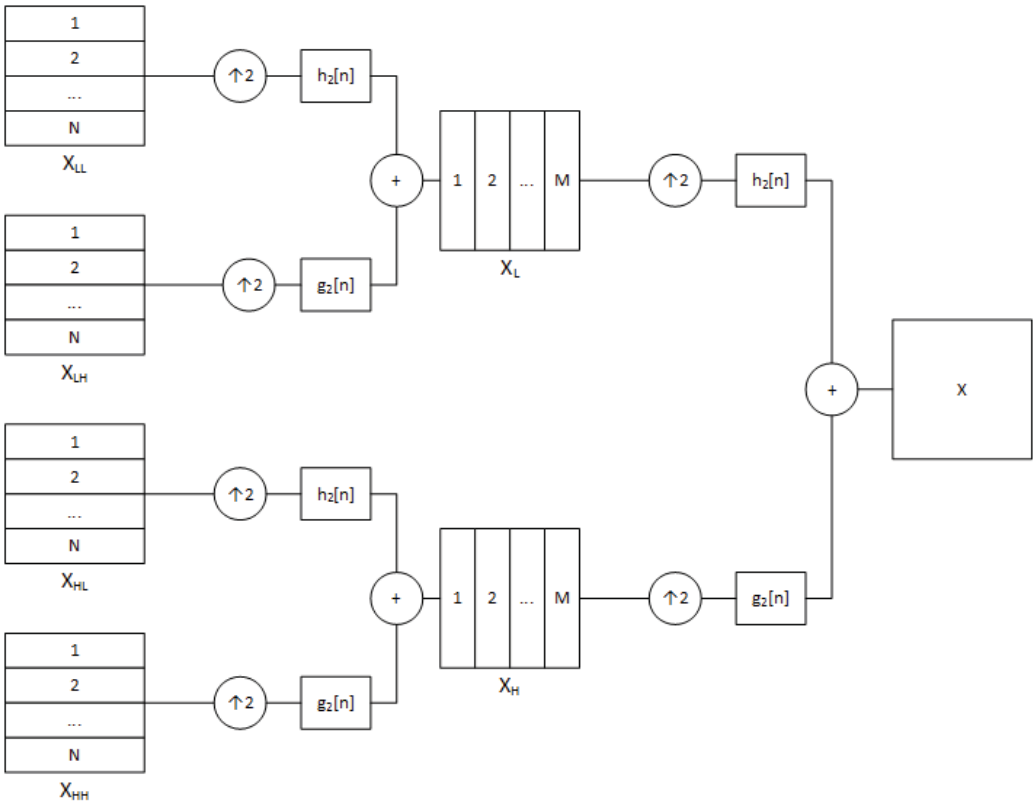

Fig. 3.6.: Two-dimensional single-level wavelet reconstruction overview

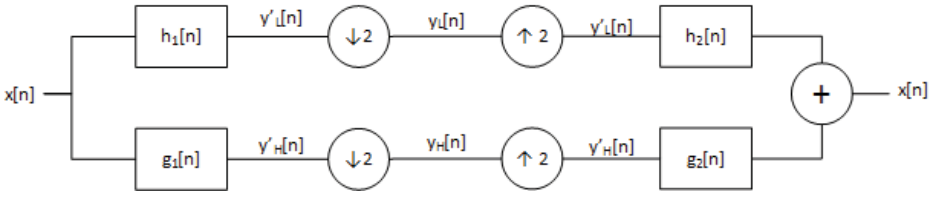

Fig. 3.7.: Perfect Reconstruction Filter Bank

3.2 Regional Variance

Within the wavelet image fusion framework described in Section 2.4, regional variance plays a key role in the fusion stage. Sometimes variance is used to choose which pixel is placed in the fused image, and other times, variance is used to define

the weights for averaging between two images. In Sections 3.2 through 3.7, both techniques are used.

Throughout this thesis, the biased estimate of the variance of a random variable X, denoted by σ_X^2, given in Equation 3.1 will be used. N represents the total number of observations of X, and μ_X is the unbiased estimate of the mean of the random variable X. The equation for μ_X is given in Equation 3.2.

$$\sigma_X^2 = \frac{1}{N}\sum_{n=1}^{N}(X(n)-\mu_X)^2 \tag{3.1}$$

$$\mu_X = \frac{1}{N}\sum_{n=1}^{N}X(n) \tag{3.2}$$

In the case of two-dimensional signals (size $N \times M$), variance estimates, denoted by $\boldsymbol{\sigma^2_X}$, will be obtained over a region R that has N' rows and M' columns ($N' << N$ and $M' << M$) centered around each point (k,l). In this thesis, estimates of the mean and variance will be referred to as regional mean and variance respectively. The equation for regional variance is provided in Equation 3.3. Using the same region defined for regional variance, the regional average, specified as $\boldsymbol{\mu_X}(k,l)$, is defined in Equation 3.4.

$$\boldsymbol{\sigma^2_X}(k,l) = \frac{1}{N'M'}\sum_{(n,m)\in R}(\boldsymbol{X}(k-n,l-m)-\boldsymbol{\mu_X}(k,l))^2 \tag{3.3}$$

$$\boldsymbol{\mu_X}(k,l) = \frac{1}{N'M'}\sum_{(n,m)\in R}\boldsymbol{X}(k-n,l-m) \tag{3.4}$$

In Sections 3.2 through 3.7, novel methods for image fusion using wavelet transforms and regional variance are presented. Throughout the remaining sections, the methods will be presented using single-level wavelet decomposition and reconstruction; however, these methods are not limited to single-level decomposition.

3.3 Regional Variance Method

In the Regional Variance method, the goal is to regional variance, as defined in Equation 3.3 to perform a weighted average between two images. Chapter 2 described a few methods that used variance in order to fuse images. The method presented in [21] uses covariance to calculate weights for the subband images for fusion while the method below uses the regional variance of individual coefficients of the subband images. In [24] and [25], variance is used on the wavelet coefficients; however, the method in which the variance is used is different than the method defined below. The method presented in [24] uses variance to select a value between two wavelet subband images, and the method presented in [25] is similar to the method below in that the variance defines a weight between the subband images for fusion. However, the way that variance is used to define the weights in [25] is different.

The Regional Variance method uses two images, $\boldsymbol{X}$ and $\boldsymbol{Y}$, as inputs, and produces a fused image $\boldsymbol{Z}$ according to the following steps:

1. Images $\boldsymbol{X}$ and $\boldsymbol{Y}$ are decomposed using a two-dimensional wavelet transform.

$$\boldsymbol{X} \stackrel{DWT}{\Longrightarrow} \begin{bmatrix} \boldsymbol{X}_{LL} & \boldsymbol{X}_{LH} \\ \boldsymbol{X}_{HL} & \boldsymbol{X}_{HH} \end{bmatrix} \tag{3.5}$$

$$\boldsymbol{Y} \stackrel{DWT}{\Longrightarrow} \begin{bmatrix} \boldsymbol{Y}_{LL} & \boldsymbol{Y}_{LH} \\ \boldsymbol{Y}_{HL} & \boldsymbol{Y}_{HH} \end{bmatrix} \tag{3.6}$$

2. The regional variance for each coefficient in the decompositions of X and Y is obtained and represented as

$$\boldsymbol{\sigma^2_X}(k,l) = \begin{bmatrix} \boldsymbol{\sigma^2}_{\boldsymbol{X}_{LL}}(k,l) & \boldsymbol{\sigma^2}_{\boldsymbol{X}_{LH}}(k,l) \\ \boldsymbol{\sigma^2}_{\boldsymbol{X}_{HL}}(k,l) & \boldsymbol{\sigma^2}_{\boldsymbol{X}_{HH}}(k,l) \end{bmatrix}$$

for each coefficient (k, l) and

$$\boldsymbol{\sigma^2_Y}(k,l) = \begin{bmatrix} \boldsymbol{\sigma^2}_{\boldsymbol{Y}_{LL}}(k,l) & \boldsymbol{\sigma^2}_{\boldsymbol{Y}_{LH}}(k,l) \\ \boldsymbol{\sigma^2}_{\boldsymbol{Y}_{HL}}(k,l) & \boldsymbol{\sigma^2}_{\boldsymbol{Y}_{HH}}(k,l) \end{bmatrix}.$$

for X and Y, respectively.

3. Weights for each coefficient at (k, l) in band $Q \in \{LL, LH, HL, HH\}$ is obtained for image X using

$$M_{\boldsymbol{X}_Q}(k,l) = \frac{{\sigma^2}_{\boldsymbol{X}_Q}(k,l)}{{\sigma^2}_{\boldsymbol{X}_Q}(k,l) + {\sigma^2}_{\boldsymbol{Y}_Q}(k,l)}. \tag{3.7}$$

The weights for the corresponding decomposition of Y is obtained as

$$M_{\boldsymbol{Y}_Q}(k,l) = 1 - M_{\boldsymbol{X}_Q}(k,l). \tag{3.8}$$

4. The subbands are fused using the weights obtained from Equations 3.7 and 3.8 via

$$\boldsymbol{Z}_Q(k,l) = \boldsymbol{X}_Q(k,l) M_{\boldsymbol{X}_Q}(k,l) + \boldsymbol{Y}_Q(k,l) M_{\boldsymbol{Y}_Q}(k,l) \tag{3.9}$$

for all (k, l) and $Q \in \{LL, LH, HL, HH\}$.

5. The inverse wavelet transform is applied using $\boldsymbol{Z}_{LL}$, $\boldsymbol{Z}_{LH}$, $\boldsymbol{Z}_{HL}$, and $\boldsymbol{Z}_{HH}$ to produce the fused image $\boldsymbol{Z}$.

In the next method, a modification is made to the Regional Variance method. Instead of treating the low-pass image in the same way that the high-pass images are processed, a different rule is applied to the LL band.

3.4 High-Pass Regional Variance Method

The High-Pass Regional Variance method is very similar to the Regional Variance method in the previous section. The main difference between the two methods is how

the LL band is treated. Instead of using regional variance, the LL images are simply averaged together on a pixel by pixel basis. Again from the two images $\boldsymbol{X}$ and $\boldsymbol{Y}$, a fused image $\boldsymbol{Z}$ is produced using the following steps:

1. $\boldsymbol{X}$ and $\boldsymbol{Y}$ are decomposed using a two-dimensional wavelet transform.
2. $\boldsymbol{X}_{LL}$ and $\boldsymbol{Y}_{LL}$ are averaged together to produce $\boldsymbol{Z}_{LL}$.

$$\boldsymbol{Z}_{LL}(k,l) = \frac{\boldsymbol{X}_{LL}(k,l) + \boldsymbol{Y}_{LL}(k,l)}{2} \tag{3.10}$$

3. The regional variance of $\boldsymbol{X}_Q$ and $\boldsymbol{Y}_Q$ where $Q \in \{LH, HL, HH\}$ is obtained.
4. The corresponding weights for $\boldsymbol{X}_Q$ and $\boldsymbol{Y}_Q$ where $Q \in \{LL, LH, HL, HH\}$ are obtained.
5. $\boldsymbol{X}_Q$ and $\boldsymbol{Y}_Q$ where $Q \in \{LH, HL, HH\}$ are fused using the weights obtained above.
6. The inverse wavelet transform is applied to $\boldsymbol{Z}_{LL}$, $\boldsymbol{Z}_{LH}$, $\boldsymbol{Z}_{HL}$, and $\boldsymbol{Z}_{HH}$ to produce the fused image $\boldsymbol{Z}$.

The next method uses a similar technique to that presented in Section 3.3;however, instead of treating each high-pass image the same way, variations of the same rule are applied to each high-pass image independently.

3.5 Directional Filtering Method

The Directional Filtering method is based on the Regional Variance method in Section 3.3 albeit different windows are utilized to obtain the regional variance of the high-pass subband images. The following procedure describes how a fused image $\boldsymbol{Z}$ is produced using Directional Filtering from X and Y.

1. Decompose $\boldsymbol{X}$ and $\boldsymbol{Y}$ using a two-dimensional wavelet transform.

2. Obtain the regional variance of $\boldsymbol{X}_{LL}$ and $\boldsymbol{Y}_{LL}$.

3. Obtain the regional variance of $\boldsymbol{X}_{LH}$ and $\boldsymbol{Y}_{LH}$ via the window orientation depicted in Figure 3.8.

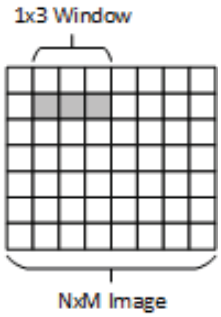

Fig. 3.8.: Window used on LH images

4. Find the regional variance of $\boldsymbol{X}_{HL}$ and $\boldsymbol{Y}_{HL}$ using using hte window configuration shown in Figure 3.9.

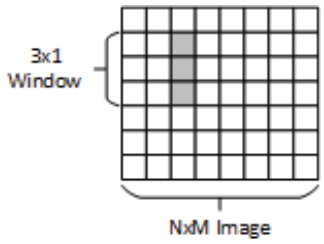

Fig. 3.9.: Window used on HL images

5. Find the regional variance of $\boldsymbol{X}_{HH}$ and $\boldsymbol{Y}_{HH}$ along the diagonals of the window shown in Figure 3.10.

6. Calculate the fusion weights for each coefficient.

7. Fuse each subband image using the weights obtained from the previous step.

8. Take the inverse wavelet transform of $\boldsymbol{Z}_{LL}$, $\boldsymbol{Z}_{LH}$, $\boldsymbol{Z}_{HL}$, and $\boldsymbol{Z}_{HH}$ to produce the fused image $\boldsymbol{Z}$.

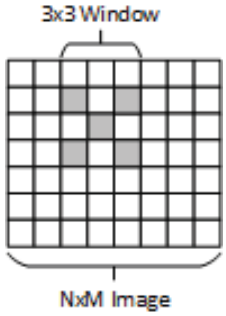

Fig. 3.10.: Window used on HH images

In the next section, another method is presented using Directional Filtering, however, as in the method in Section 3.4, the LL image is treated independently from the high-pass images. Additionally, a threshold is applied to assist with decisions in the high-pass images.

3.6 High-Pass Directional Filtering with Thresholding Method

The High-Pass Directional Filtering with Thresholding method differs from the Directional Filtering method in Section 3.5 by altering how the LL image is handled. In addition to treating the LL image independently, this new method also introduces a threshold to make decisions between the input images. The subsequent steps describe the High-Pass Directional Filtering with Thresholding method:

1. Decompose $\boldsymbol{X}$ and $\boldsymbol{Y}$ using a two-dimensional wavelet transform.
2. Average $\boldsymbol{X}_{LL}$ and $\boldsymbol{Y}_{LL}$.
3. Obtain the regional variance of $\boldsymbol{X}_{LH}$ and $\boldsymbol{Y}_{LH}$ using the window given in Figure 3.8.
4. Find the regional variance of $\boldsymbol{X}_{HL}$ and $\boldsymbol{Y}_{HL}$ using the window depicted in Figure 3.9.

5. Obtain the regional variance of $\boldsymbol{X}_{HH}$ and $\boldsymbol{Y}_{HH}$ using the diagonal shaped window given in Figure 3.10.

6. Calculate the fusion weights for each coefficient in subband Q where $Q \in \{LH, HL, HH\}$.

7. Fuse $\boldsymbol{X}_Q$ and $\boldsymbol{Y}_Q$ using a threshold T and the following:

$$\boldsymbol{Z}_Q(k,l) = \begin{cases} \boldsymbol{X}_Q(k,l) & if M_{\boldsymbol{X}_Q}(k,l) > T \\ \boldsymbol{Y}_Q(k,l) & if M_{\boldsymbol{Y}_Q}(k,l) > T \\ \boldsymbol{X}_Q(k,l)M_{\boldsymbol{X}_Q}(k,l) + \boldsymbol{Y}_Q(k,l)M_{\boldsymbol{Y}_Q}(k,l) & \text{otherwise} \end{cases} \tag{3.11}$$

   where $Q \in \{LH, HL, HH\}$.

8. Take the inverse wavelet transform of $\boldsymbol{Z}_{LL}$, $\boldsymbol{Z}_{LH}$, $\boldsymbol{Z}_{HL}$, and $\boldsymbol{Z}_{HH}$ to produce the fused image $\boldsymbol{Z}$.

The next method is similar to the current method in that wavelets, regional variance, and thresholding are used throughout the method. However, a different approach is taken when applying the threshold in the fusion process.

3.7 Directional Filtering with an Adaptive Threshold Method

The final method proposed in this thesis is based on Directional Filtering. Again, the method uses wavelets, regional variance, and threholding, but the implementation of the threshold in the method is different than the previous method. The procedure to obtaining a fused image Z from input images X and Y is as follows:

1. Decompose $\boldsymbol{X}$ and $\boldsymbol{Y}$ using a two-dimensional wavelet transform.

2. Obtain the regional variance of $\boldsymbol{X}_{LL}$ and $\boldsymbol{Y}_{LL}$ using a rectangular window.

3. Find the regional variance of $\boldsymbol{X}_{LH}$ and $\boldsymbol{Y}_{LH}$ using the window in Figure 3.8.

4. Obtain the regional variance of $\boldsymbol{X}_{HL}$ and $\boldsymbol{Y}_{HL}$ using the window in Figure 3.9.

5. Find the regional variance of $\boldsymbol{X}_{HH}$ and $\boldsymbol{Y}_{HH}$ along the diagonals of the window given in Figure 3.10.

6. Calculate the fusion weights for X_Q and Y_Q where $Q \in \{LL, LH, HL, HH\}$.

7. Fuse each image given a threshold T where $T \in (0.5, 1)$ using

$$\boldsymbol{Z}_Q(k,l) = \begin{cases} T\boldsymbol{X}_Q(k,l) + (1-T)\boldsymbol{Y}_Q(k,l) & \text{if } M_{\boldsymbol{X}_Q}(k,l) \geq T \\ (1-T)\boldsymbol{X}_Q(k,l) + T\boldsymbol{Y}_Q(k,l) & \text{if } M_{\boldsymbol{Y}_Q}(k,l) \geq T \\ \boldsymbol{X}_Q(k,l)M_{\boldsymbol{X}_Q}(k,l) + \boldsymbol{Y}_Q(k,l)M_{\boldsymbol{Y}_Q}(k,l) & \text{otherwise} \end{cases} . \tag{3.12}$$

8. Take the inverse wavelet transform of $\boldsymbol{Z}_{LL}$, $\boldsymbol{Z}_{LH}$, $\boldsymbol{Z}_{HL}$, and $\boldsymbol{Z}_{HH}$ to produce the fused image $\boldsymbol{Z}$.

In this chapter, five methods have been presented. Each method presented is a novel approach to image fusion using a combination of regional variance and wavelet transforms. The novelty for each method comes from method in which regional variance is used to calculate weights for each wavelet subband. In addition, the concept of directional filtering used in the last three methods is also a novel feature. In the next chapter, results of each method will be shown and discussed in detail.

4. RESULTS

In Chapter 3, five novel methods for image fusion were presented. Throughout this chapter, results for each method will be presented. In Section 4.1, the group of images used to test each method will be presented followed by a presentation of commonly used fusion method to be compared to the proposed methods in Section 4.2. Sections 4.3 through 4.7 will present results for each method and compare the performance to the methods presented in Section 4.2. Finally, Section 4.8 will discuss the performance of each method in relation to the others.

4.1 Data Set

In order to present and analyze the performance of each proposed method, a set of eleven images was utilized. The images come from two data sources. The first set of images used was provided by NSWC Crane. The second set of images was provided by [32] and contains a collection of images from different sources including TNO, The Netherlands and David Dwyer of Octec Ltd. The images from both sets are given in Figures 4.1 through 4.11.

(a) Visible Image (b) Infrared Image

Fig. 4.1.: Set 1 images provided by NSCW Crane

(a) Visible Image (b) Infrared Image

Fig. 4.2.: Set 2 images provided by NSCW Crane

(a) Visible Image (b) Infrared Image

Fig. 4.3.: Set 3 images provided by NSCW Crane

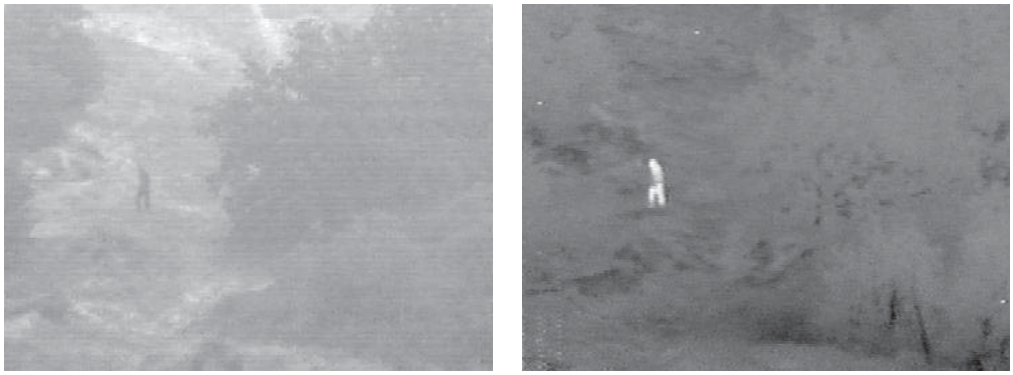

(a) Visible Image (b) Infrared Image

Fig. 4.4.: Set 4 images provided by [32]

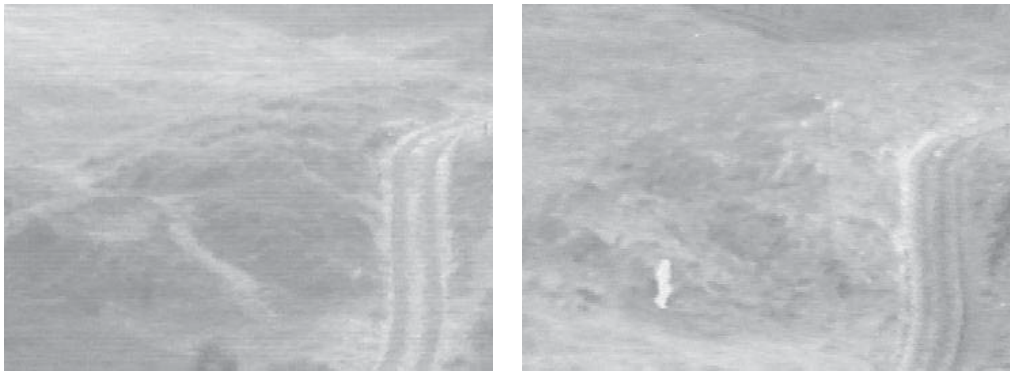

(a) Visible Image (b) Infrared Image

Fig. 4.5.: Set 5 images provided by [32]

(a) Visible Image (b) Infrared Image

Fig. 4.6.: Set 6 images provided by [32]

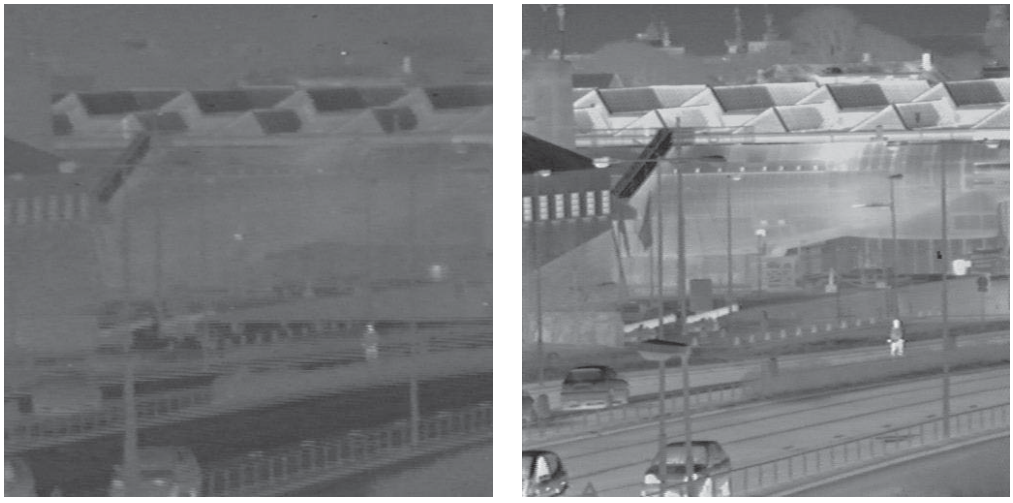

(a) Visible Image (b) Infrared Image

Fig. 4.7.: Set 7 images provided by [32]

(a) Visible Image (b) Infrared Image

Fig. 4.8.: Set 8 images provided by [32]

(a) Visible Image (b) Infrared Image

Fig. 4.9.: Set 9 images provided by [32]

(a) Visible Image (b) Infrared Image

Fig. 4.10.: Set 10 images provided by [32]

(a) Visible Image (b) Infrared Image

Fig. 4.11.: Set 11 images provided by [32]

4.2 Method Evaluation

Using the images shown in Section 4.1, each method discussed in Chapter 3 was tested. Additionally, some commonly used methods were also used on the data sets in order to establish a base case to compare the proposed methods. Furthermore a evaluation of each method will be provided in terms of the entropy of each fused image [25].

4.2.1 Entropy

While the use of entropy can provide a good quantitative measure of information within an image, the quality of the fused image also plays an important role in the success of an image fusion method.

To estimate the entropy of an image $\boldsymbol{X}$, the first step is to generate a histogram of the values of $\boldsymbol{X}$, denoted as $p_{\boldsymbol{X}}$. Once the histogram is obtained, the entropy, $H_{\boldsymbol{X}}$, is estimated using

$$H_{\boldsymbol{X}} = -\sum_{i=0}^{L-1} p_{\boldsymbol{X}}(i) \log_2 p_{\boldsymbol{X}}(i). \tag{4.1}$$

where L is the number of bins in the histogram. For a grayscale image, the number of bins is typically 256. The subsequent sections introduce commonly used fusion methods.

Now that the concept of entropy has been introduced, the four sections will focus on basic fusion methods that will be used to compare against the proposed methods in Chapter 3. The base methods and their results are presented in Sections 4.2.2 through 4.2.5.

4.2.2 Greatest Pixel Value Based Fusion

The Greatest Pixel method is one of the most basic methods for image fusion. Given two images, $\boldsymbol{X}$ and $\boldsymbol{Y}$, the Greatest Pixel method produces a new image $\boldsymbol{Z}$ by

selecting the greatest value from $\boldsymbol{X}$ or $\boldsymbol{Y}$ for each pixel (k, l). Mathematically, the greatest pixel method is represented as

$$\boldsymbol{Z}(k,l) = \begin{cases} \boldsymbol{X}(k,l) & \text{if } \boldsymbol{X}(k,l) \geq \boldsymbol{Y}(k,l) \\ \boldsymbol{Y}(k,l) & \text{if } \boldsymbol{X}(k,l) < \boldsymbol{Y}(k,l) \end{cases} \tag{4.2}$$

The results of this method on the images in Figures 4.1 through 4.11 can been seen in Figure 4.12 through 4.22.

Fig. 4.12.: The result of applying the Greatest Pixel method to the images in Figure 4.1

Fig. 4.13.: The result of applying the Greatest Pixel method to the images in Figure 4.2

Fig. 4.14.: The result of applying the Greatest Pixel method to the images in Figure 4.3

Fig. 4.15.: The result of applying the Greatest Pixel method to the images in Figure 4.4

Fig. 4.16.: The result of applying the Greatest Pixel method to the images in Figure 4.5

Fig. 4.17.: The result of applying the Greatest Pixel method to the images in Figure 4.6

Fig. 4.18.: The result of applying the Greatest Pixel method to the images in Figure 4.7

Fig. 4.19.: The result of applying the Greatest Pixel method to the images in Figure 4.8

Fig. 4.20.: The result of applying the Greatest Pixel method to the images in Figure 4.9

Fig. 4.21.: The result of applying the Greatest Pixel method to the images in Figure 4.10

Fig. 4.22.: The result of applying the Greatest Pixel method to the images in Figure 4.11

Instead of choosing the maximum pixel value between two images, the next method presented is based on averaging the two images.

4.2.3 Pixel Averaging

In the Pixel Averging method, an average is taken of the two images. Given two input images, $\boldsymbol{X}$ and $\boldsymbol{Y}$, the fused image $\boldsymbol{Z}$ is produced by applying Equation 4.3 to each pixel (k, l).

$$\boldsymbol{Z} = \frac{1}{2}(\boldsymbol{X} + \boldsymbol{Y}) \tag{4.3}$$

The results of this method can be seen in Figures 4.23 through 4.33.

4.2.4 Wavelet Greatest Pixel

In the previous two sections, simple methods that work in the original spatial domain have been presented. This next method is an adaptation of the method presented in Section 4.2.2 by applying a wavelet transform.

Fig. 4.23.: The result of applying the Pixel Averging method to the images in Figure 4.1

Fig. 4.24.: The result of applying the Pixel Averging method to the images in Figure 4.2

In particular, the two input images, $\boldsymbol{X}$ and $\boldsymbol{Y}$, are decomposed using wavelet transforms to produce $\boldsymbol{X}_{LL}$, $\boldsymbol{X}_{LH}$, $\boldsymbol{X}_{HL}$, and $\boldsymbol{X}_{HH}$ from $\boldsymbol{X}$ and $\boldsymbol{Y}_{LL}$, $\boldsymbol{Y}_{LH}$, $\boldsymbol{Y}_{HL}$, and $\boldsymbol{Y}_{HH}$ from $\boldsymbol{Y}$ respectively. Using Equation 4.2, $\boldsymbol{Z}_{LL}$, $\boldsymbol{Z}_{LH}$, $\boldsymbol{Z}_{HL}$, and $\boldsymbol{Z}_{HH}$ are generated from the subband images of $\boldsymbol{X}$ and $\boldsymbol{Y}$. Finally, a inverse wavelet transform

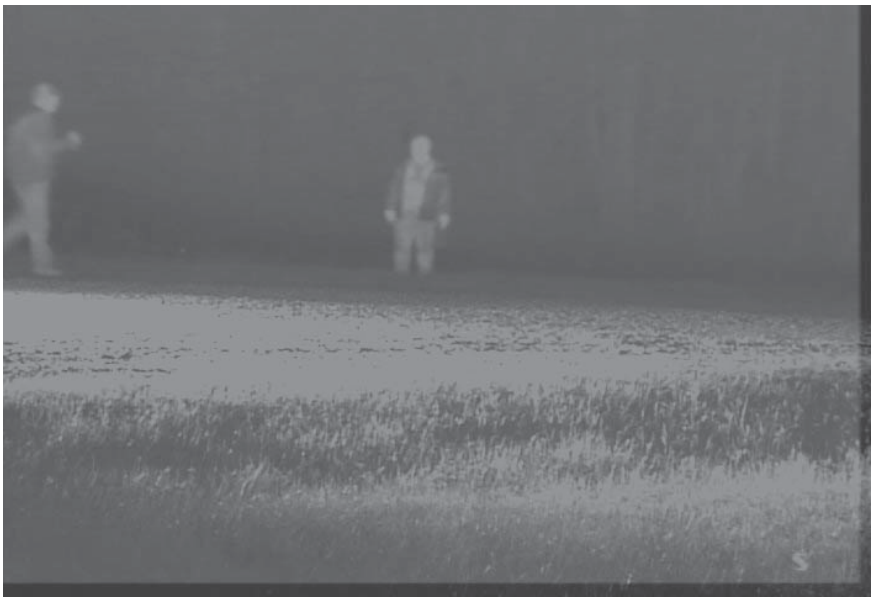

Fig. 4.25.: The result of applying the Pixel Averging method to the images in Figure 4.3

Fig. 4.26.: The result of applying the Pixel Averging method to the images in Figure 4.4

Fig. 4.27.: The result of applying the Pixel Averging method to the images in Figure 4.5

Fig. 4.28.: The result of applying the Pixel Averging method to the images in Figure 4.6

Fig. 4.29.: The result of applying the Pixel Averging method to the images in Figure 4.7

Fig. 4.30.: The result of applying the Pixel Averging method to the images in Figure 4.8

Fig. 4.31.: The result of applying the Pixel Averging method to the images in Figure 4.9

Fig. 4.32.: The result of applying the Pixel Averging method to the images in Figure 4.10

Fig. 4.33.: The result of applying the Pixel Averging method to the images in Figure 4.11

creates the final image $\boldsymbol{Z}$ from $\boldsymbol{Z}_{LL}$, $\boldsymbol{Z}_{LH}$, $\boldsymbol{Z}_{HL}$, and $\boldsymbol{Z}_{HH}$. The results of this method can be seen in Figure 4.34 through 4.44.

Fig. 4.34.: The result of applying the Wavelet Greatest Pixel method to the images in Figure 4.1

Fig. 4.35.: The result of applying the Wavelet Greatest Pixel method to the images in Figure 4.2

Fig. 4.36.: The result of applying the Wavelet Greatest Pixel method to the images in Figure 4.3

Fig. 4.37.: The result of applying the Wavelet Greatest Pixel method to the images in Figure 4.4

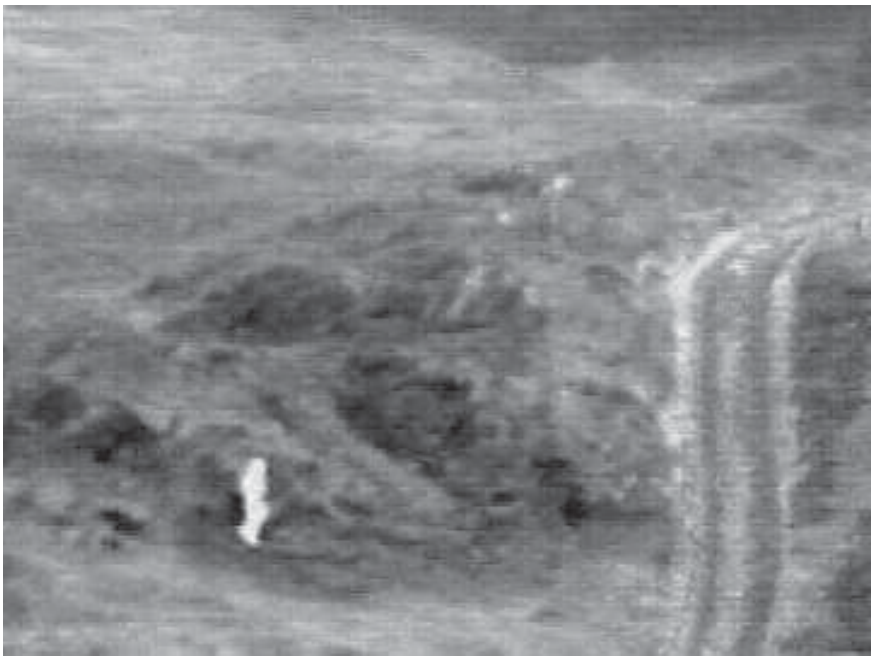

Fig. 4.38.: The result of applying the Wavelet Greatest Pixel method to the images in Figure 4.5

Fig. 4.39.: The result of applying the Wavelet Greatest Pixel method to the images in Figure 4.6

Fig. 4.40.: The result of applying the Wavelet Greatest Pixel method to the images in Figure 4.7

Fig. 4.41.: The result of applying the Wavelet Greatest Pixel method to the images in Figure 4.8

Fig. 4.42.: The result of applying the Wavelet Greatest Pixel method to the images in Figure 4.9

Fig. 4.43.: The result of applying the Wavelet Greatest Pixel method to the images in Figure 4.10

Fig. 4.44.: The result of applying the Wavelet Greatest Pixel method to the images in Figure 4.11

4.2.5 Wavelet Average

In Section 4.2.3, a method for averaging two images together was presented. In this section, the averaging method is applied to wavelet coefficients.

Again, the input images, $\boldsymbol{X}$ and $\boldsymbol{Y}$, are decomposed to produce $\boldsymbol{X}_{LL}$, $\boldsymbol{X}_{LH}$, $\boldsymbol{X}_{HL}$, and $\boldsymbol{X}_{HH}$ from $\boldsymbol{X}$ and $\boldsymbol{Y}_{LL}$, $\boldsymbol{Y}_{LH}$, $\boldsymbol{Y}_{HL}$, and $\boldsymbol{Y}_{HH}$ from $\boldsymbol{Y}$. Using Equation 4.3, $\boldsymbol{Z}_{LL}$, $\boldsymbol{Z}_{LH}$, $\boldsymbol{Z}_{HL}$, and $\boldsymbol{Z}_{HH}$ are generated from $\boldsymbol{X}_{LL}$, $\boldsymbol{X}_{LH}$, $\boldsymbol{X}_{HL}$, $\boldsymbol{X}_{HH}$, $\boldsymbol{Y}_{LL}$, $\boldsymbol{Y}_{LH}$, $\boldsymbol{Y}_{HL}$, and $\boldsymbol{Y}_{HH}$. The final step involves reconstructing the fused image $\boldsymbol{Z}$ from $\boldsymbol{Z}_{LL}$, $\boldsymbol{Z}_{LH}$, $\boldsymbol{Z}_{HL}$, and $\boldsymbol{Z}_{HH}$ via an inverse wavelet transform. The results for Wavelet Average can be seen in Figure 4.45 through 4.55.

Fig. 4.45.: The result of applying the Wavelet Average method to the images in Figure 4.1

The final basic method will be presented in the next section. Like the previous two methods, the next method utilizes wavelet transforms for fusion. However, instead of choosing the largest coefficient value or averging, variance is used to make a selection between wavelet coefficents.

Fig. 4.46.: The result of applying the Wavelet Average method to the images in Figure 4.2

Fig. 4.47.: The result of applying the Wavelet Average method to the images in Figure 4.3

Fig. 4.48.: The result of applying the Wavelet Average method to the images in Figure 4.4

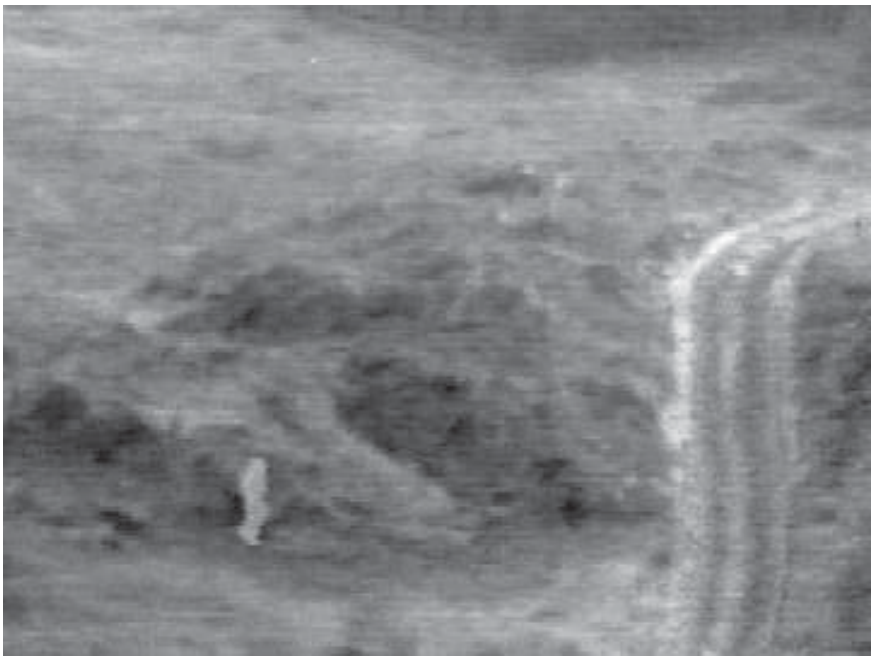

Fig. 4.49.: The result of applying the Wavelet Average method to the images in Figure 4.5

Fig. 4.50.: The result of applying the Wavelet Average method to the images in Figure 4.6

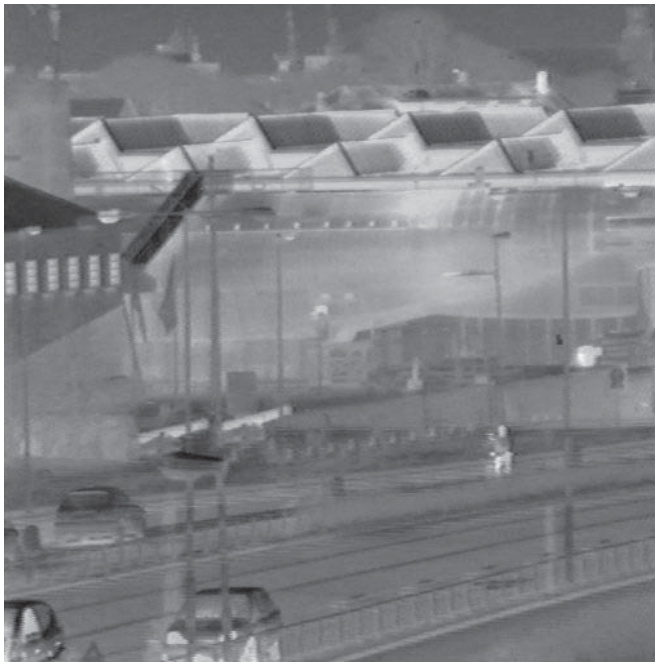

Fig. 4.51.: The result of applying the Wavelet Average method to the images in Figure 4.7

Fig. 4.52.: The result of applying the Wavelet Average method to the images in Figure 4.8

Fig. 4.53.: The result of applying the Wavelet Average method to the images in Figure 4.9

Fig. 4.54.: The result of applying the Wavelet Average method to the images in Figure 4.10

Fig. 4.55.: The result of applying the Wavelet Average method to the images in Figure 4.11

4.2.6 Wavelet Variance Selection

In Chapter 2, a variance based method was introduced in [24]. Using regional variance, decisions are made between the high-pass subbands of the wavelet decomposed input images. For two input images, $\boldsymbol{X}$ and $\boldsymbol{Y}$, wavelet decomposition is applied to produce $\boldsymbol{X}_{LL}$, $\boldsymbol{X}_{LH}$, $\boldsymbol{X}_{HL}$, and $\boldsymbol{X}_{HH}$ from $\boldsymbol{X}$ and $\boldsymbol{Y}_{LL}$, $\boldsymbol{Y}_{LH}$, $\boldsymbol{Y}_{HL}$, and $\boldsymbol{Y}_{HH}$ from $\boldsymbol{Y}$. $\boldsymbol{X}_{LL}$ and $\boldsymbol{Y}_{LL}$ are averaged together pixel-by-pixel. For each high-pass subband image Q where $Q \in \{LH, HL, HH\}$, the following equation defines how wavelet coefficients are selected:

$$\boldsymbol{Z}_Q(k,l) = \begin{cases} \boldsymbol{X}_Q(k,l) & \text{if } \boldsymbol{\sigma^2}_{\boldsymbol{X}_Q}(k,l) \geq \boldsymbol{\sigma^2}_{\boldsymbol{Y}_Q}(k,l) \\ \boldsymbol{Y}_Q(k,l) & \text{if } \boldsymbol{\sigma^2}_{\boldsymbol{X}_Q}(k,l) < \boldsymbol{\sigma^2}_{\boldsymbol{Y}_Q}(k,l) \end{cases} . \tag{4.4}$$

The results of the Wavelet Variance Method are presented in Figures 4.56 through 4.66

Fig. 4.56.: The result of applying the Wavelet Variance Selection method to the images in Figure 4.1

Fig. 4.57.: The result of applying the Wavelet Variance Selection method to the images in Figure 4.2

Fig. 4.58.: The result of applying the Wavelet Variance Selection method to the images in Figure 4.3

Fig. 4.59.: The result of applying the Wavelet Variance Selection method to the images in Figure 4.4

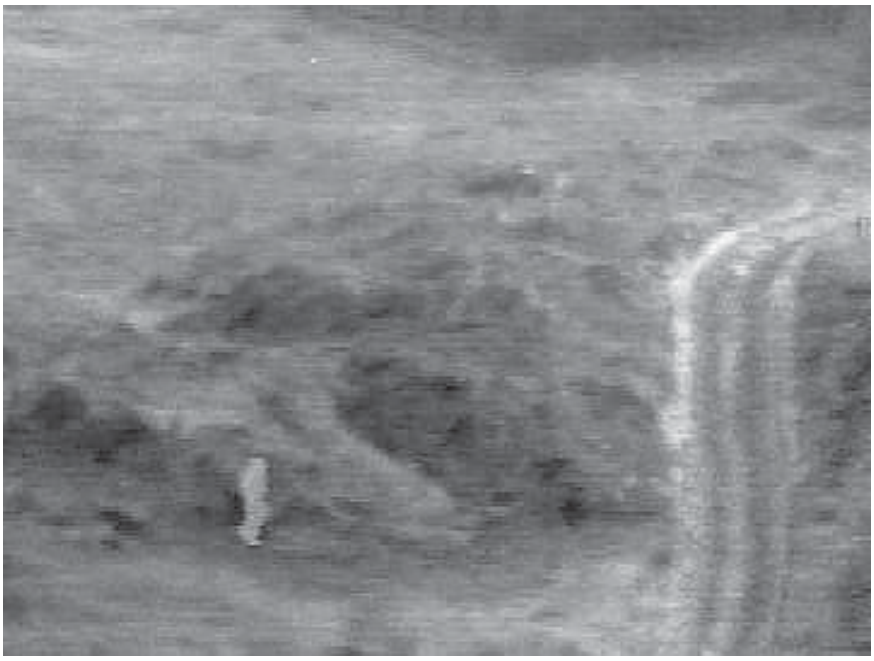

Fig. 4.60.: The result of applying the Wavelet Variance Selection method to the images in Figure 4.5

Fig. 4.61.: The result of applying the Wavelet Variance Selection method to the images in Figure 4.6

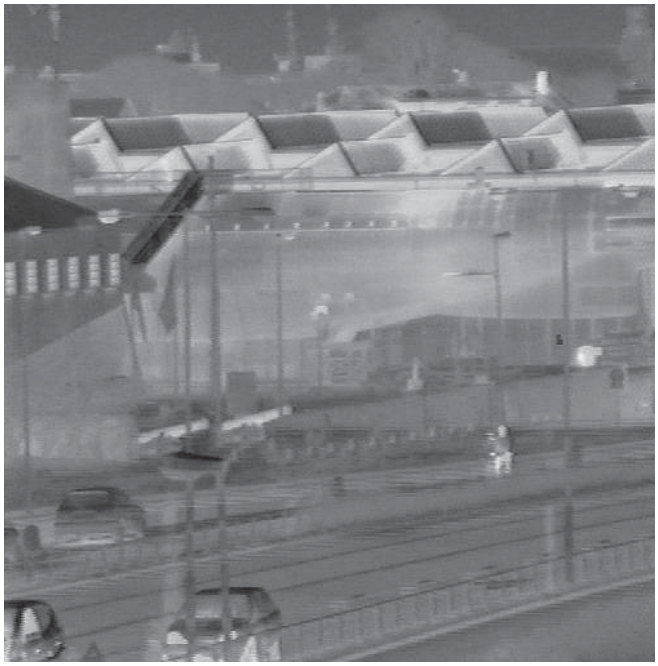

Fig. 4.62.: The result of applying the Wavelet Variance Selection method to the images in Figure 4.7

Fig. 4.63.: The result of applying the Wavelet Variance Selection method to the images in Figure 4.8

Fig. 4.64.: The result of applying the Wavelet Variance Selection method to the images in Figure 4.9

Fig. 4.65.: The result of applying the Wavelet Variance Selection method to the images in Figure 4.10

Fig. 4.66.: The result of applying the Wavelet Variance Selection method to the images in Figure 4.11

In order to compare the results of the proposed methods to the base methods, the entropy of each outcome of each base method is presented in Table 4.1.

Among the common methods, the best performances visually and in terms of entropy came from the wavelet transform based methods. With the Greatest Pixel and Pixel Averging methods, much of the visual quality was lost in the fused image

Table 4.1: Entropy values of each image presented in Figures 4.12 through 4.55

Entropy Results					
Set	**Greatest Pixel**	**Pixel Averging**	**Wavelet Greatest Pixel**	**Wavelet Average**	**Wavelet Variance Selection**
Set 1	5.307	5.480	5.577	5.760	5.806
Set 2	5.334	5.421	5.716	6.424	6.672
Set 3	5.885	5.572	6.217	6.707	6.622
Set 4	6.132	2.755	6.836	6.500	6.476
Set 5	6.014	2.439	7.233	6.771	7.099
Set 6	5.758	4.543	6.008	5.453	5.313
Set 7	6.859	5.964	7.063	6.876	6.921
Set 8	6.758	5.832	6.549	5.935	5.727
Set 9	6.031	5.224	6.428	6.678	6.411
Set 10	6.506	4.691	6.783	6.882	6.567
Set 11	6.609	4.182	6.970	6.964	6.626

and entropy values were consistently less than the wavelet based methods. In many cases, the important details in both images were diminished when fusing with the non-wavelet based methods. When working with an image set where either the visible or infrared images dominated the content, the Wavelet Greatest Pixel method performed well visually and in terms of entropy; although, in situations where objects in both input images are clearly defined, some of the important details were masked by the Wavelet Greatest Pixel method. The Wavelet Average method, on the other hand, objects were well defined in both input images. However, when one input image clearly defined an object, and the same object was indiscernible in the second input image, the Wavelet Average method had poor performance. Out of the three wavelet based methods, the Wavelet Variance Selection method was the best visually; however, since the LL subbands are averaged, the overall contrast of the fused image was reduced.

Now that each base method has been discussed, the upcoming sections will discuss the results of each method on the input images that were presented in Section 4.1. Each method will be compared to the results produced by the base methods discussed in Sections 4.2.2 through 4.2.5.

4.3 Regional Variance Method Results

The results of the Regional Variance method are depicted in Figures 4.67 through 4.77 for the images in Figures 4.1 through 4.11 based on a 3×3 window and two levels of wavelet decomposition that were found to provide the "best" performance. The entropy values for each image are provided in Table 4.2.

Fig. 4.67.: The result of applying the Regional Variance method to the images in Figure 4.1

Based on the result of Tables Table 4.1 and 4.2, the Regional Variance method performs as well or better than some of base methods. Against the Pixel Averging method, the Regional Variance method's entropy results are consistently greater. However, compared to the other four methods, Regional Variance only outperforms them some of the time. For example, the Wavelet Greatest Pixel method is better in terms of entropy on the images from Figures 4.4 and 4.8 images, and for images from Figure 4.2, the Wavelet Average method seems to outperform the Regional Variance method in terms of entropy. Compared against the Wavelet Variance Selection method, the Regional Variance method has similar or better performance in terms of entropy. While there are a few cases where the Wavelet Variance Selection method has higher entropy values than the Regional Variance method, the Regional Variance method has similar or better performance in most cases.

Fig. 4.68.: The result of applying the Regional Variance method to the images in Figure 4.2

Fig. 4.69.: The result of applying the Regional Variance method to the images in Figure 4.3

Fig. 4.70.: The result of applying the Regional Variance method to the images in Figure 4.4

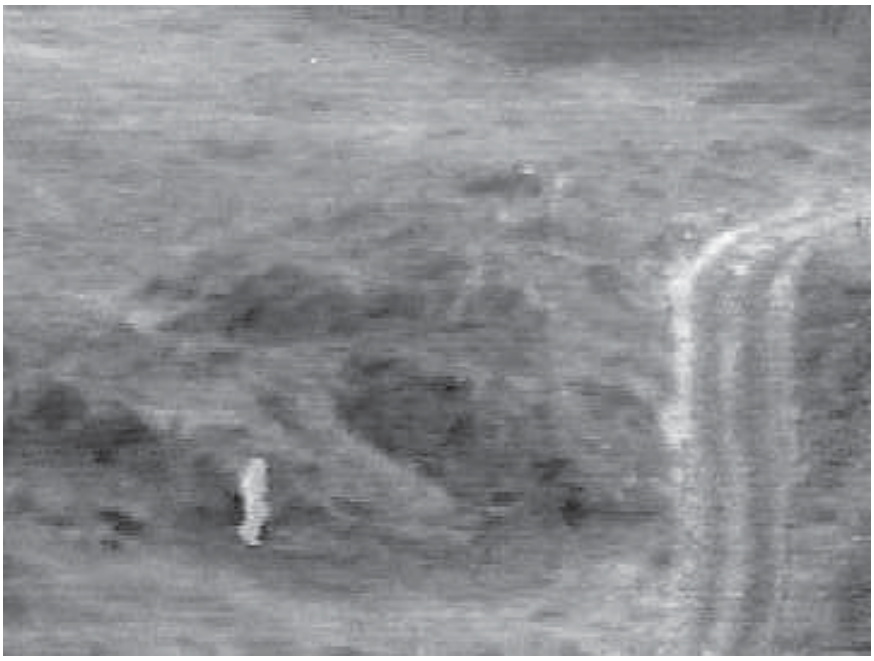

Fig. 4.71.: The result of applying the Regional Variance method to the images in Figure 4.5

Fig. 4.72.: The result of applying the Regional Variance method to the images in Figure 4.6

Fig. 4.73.: The result of applying the Regional Variance method to the images in Figure 4.7

Fig. 4.74.: The result of applying the Regional Variance method to the images in Figure 4.8

Fig. 4.75.: The result of applying the Regional Variance method to the images in Figure 4.9

Fig. 4.76.: The result of applying the Regional Variance method to the images in Figure 4.10

Fig. 4.77.: The result of applying the Regional Variance method to the images in Figure 4.11

Table 4.2: Entropy values of the images displayed in Figures 4.67 through 4.77

Entropy Results	
Set	**Regional Variance**
Set 1	5.861
Set 2	5.980
Set 3	6.429
Set 4	6.442
Set 5	7.108
Set 6	6.144
Set 7	6.866
Set 8	6.280
Set 9	6.324
Set 10	6.547
Set 11	6.541

From a visual quality stand point, the Regional Variance does well in some cases but not in others. In the first two images from Figures 4.67 and 4.68, much of image is not very sharp. Many of the details were lost, mainly due to the level of noise present in the visible images. However, on images where there is a lower amount of noise in the visible image, like those in Figures 4.69 through 4.77, and an abundance of detail, the Regional Variance method is well suited. One of the issues with Greatest Pixel, Wavelet Average, Wavelet Greatest Pixel, and Wavelet Variance Selection is the overall reduction in contrast. With both averaging methods and Wavelet Variance Selection, the overall image becomes very dark, and with Wavelet Greatest Pixel, the images seem to be very bright. The benefit of the Regional Variance method is the preservation of contrast.

Now that the Regional Variance method's results have been presented and compared to the base methods, the results of the High-Pass Regional Variance method will be discussed. The difference between the Regional Variance method and the High-Pass Regional Variance method is how the LL band is handled. Instead of using regional variance, the LL bands are averaged together.

4.4 High-Pass Regional Variance Results

In this section, the results of the High-Pass Regional Variance method are provided and compared to the base methods presented in Section 4.2. Again, the main difference between this method and the Regional Variance method is that the LL images are averaged together rather than using regional variance. Using a 3×3 window for regional variance and two levels of wavelet decomposition, the image results for the High-Pass Regional Variance method are presented in Figures 4.78 through 4.88.

Fig. 4.78.: The result of applying the High-Pass Regional Variance method to the images in Figure 4.1

Similar to the Regional Variance Method, the High-Pass Regional Variance method performs well in some of the cases but poorly in others. Looking at the Wavelet Greatest Pixel and Wavelet Average methods, the two strongest base methods for image fusion, the High-Pass Regional Variance method out performs about half the time. From comparing Table 4.3 with Table 4.1, the High-Pass Regional Variance method out performs the Wavelet Average method most of the time, and when the Wavelet Average method seems to do better, the difference between entropy values produced by the two methods is small. In reference to the Wavelet Variance Selection method, the High-Pass Regional Variance method has a similar performance. While the en-

Fig. 4.79.: The result of applying the High-Pass Regional Variance method to the images in Figure 4.2

Fig. 4.80.: The result of applying the High-Pass Regional Variance method to the images in Figure 4.3

Fig. 4.81.: The result of applying the High-Pass Regional Variance method to the images in Figure 4.4

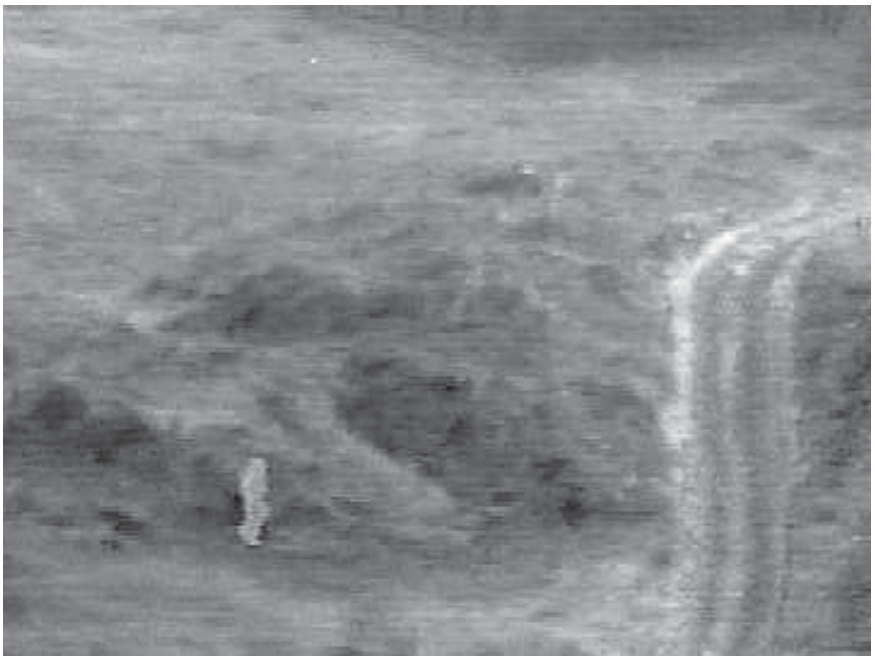

Fig. 4.82.: The result of applying the High-Pass Regional Variance method to the images in Figure 4.5

Fig. 4.83.: The result of applying the High-Pass Regional Variance method to the images in Figure 4.6

Fig. 4.84.: The result of applying the High-Pass Regional Variance method to the images in Figure 4.7

Fig. 4.85.: The result of applying the High-Pass Regional Variance method to the images in Figure 4.8

Fig. 4.86.: The result of applying the High-Pass Regional Variance method to the images in Figure 4.9

Fig. 4.87.: The result of applying the High-Pass Regional Variance method to the images in Figure 4.10

Fig. 4.88.: The result of applying the High-Pass Regional Variance method to the images in Figure 4.11

Table 4.3: Entropy values of the images displayed in Figures 4.78 through 4.88

Entropy Results	
Set	**High-Pass Regional Variance**
Set 1	5.869
Set 2	6.681
Set 3	6.126
Set 4	6.351
Set 5	7.065
Set 6	5.426
Set 7	6.713
Set 8	5.660
Set 9	6.294
Set 10	6.220
Set 11	6.242

tropy of the High-Pass Regional Variance method is sightly less than the Wavelet Variance Selection method, the entropy values are very similar.

Since the High-Pass Regional Variance method utilizes averaging of the LL band, some of the results of and High-Pass Regional Variance methods appear to be very similar to the Wavelet Average and Wavelet Variance Selection methods. For instance, the images in Figures 4.46 and 4.79 look identical. Even though the entropy of the High-Pass Regional Variance Method is higher, the visual quality is difficult to distinguish. In fact, many of the methods that use averaging on the LL band have very similar qualities to the Wavelet Average method.

In the next section, the results of Directional Filtering will be presented and compared to the base methods. Directional Filtering is similar to the Regional Variance method with modifications to the window shapes based on the band that is being processed.

4.5 Directional Filtering Results

The results of the Directional Filtering method will be presented throughout this section. Like the Regional Variance method, the Directional Filtering method uses regional variance on all bands of the wavelet decomposed images; however, the window shapes are adapted for each high-pass image. Using the base methods presented in Section 4.2 for comparison, the Directional Filtering method will be compared quantitatively and qualitatively. Results of the Directional Filtering Method are shown in Figures 4.89 through 4.99.

Fig. 4.89.: The result of applying the Directional Filtering method to the images in Figure 4.1

By comparing the entropy values in Table 4.4 and Table 4.1, it is observed that the performance of the Directional Filtering method is dependent on the amount of noise present in the input images. The results in Table 4.4 are very similar to the results of the Regional Variance Method presented in Table 4.2.

Because the results of the Directional Filtering method are similar to the results of the Regional Variance method, the relationship between the Directional Filtering method and the Wavelet Variance Selection method is the same for the relationship between the Regional Variance method and the Wavelet Variance Selection method. Directional Filtering usual has similar or better performance in terms of entropy.

Fig. 4.90.: The result of applying the Directional Filtering method to the images in Figure 4.2

Fig. 4.91.: The result of applying the Directional Filtering method to the images in Figure 4.3

Fig. 4.92.: The result of applying the Directional Filtering method to the images in Figure 4.4

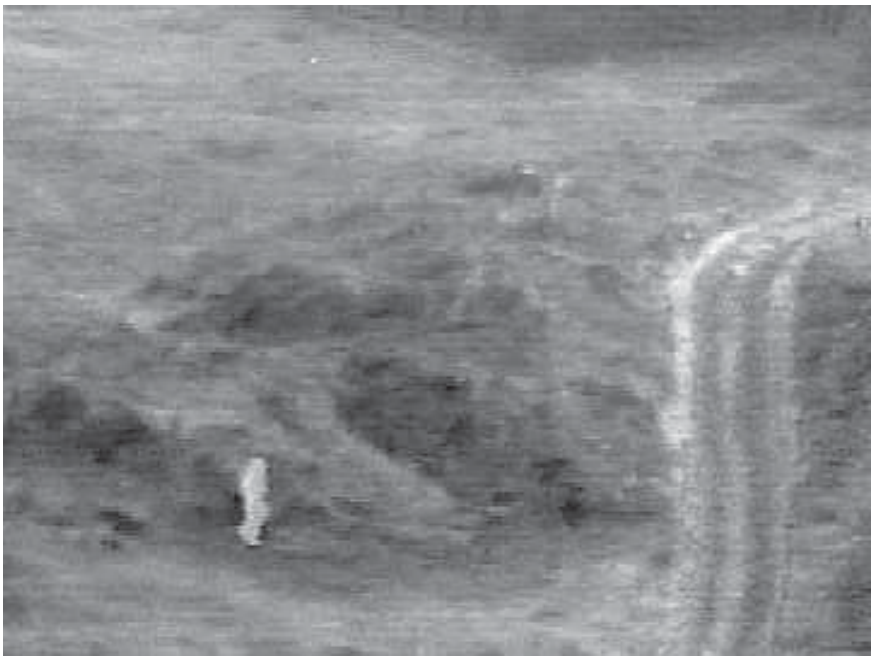

Fig. 4.93.: The result of applying the Directional Filtering method to the images in Figure 4.5

Fig. 4.94.: The result of applying the Directional Filtering method to the images in Figure 4.6

Fig. 4.95.: The result of applying the Directional Filtering method to the images in Figure 4.7

Fig. 4.96.: The result of applying the Directional Filtering method to the images in Figure 4.8

Fig. 4.97.: The result of applying the Directional Filtering method to the images in Figure 4.9

Fig. 4.98.: The result of applying the Directional Filtering method to the images in Figure 4.10

Fig. 4.99.: The result of applying the Directional Filtering method to the images in Figure 4.11

Table 4.4: Entropy values of the images displayed in Figures 4.89 through 4.99

Entropy Results	
Set	**Directional Filtering**
Set 1	5.859
Set 2	5.980
Set 3	6.459
Set 4	6.420
Set 5	7.098
Set 6	6.127
Set 7	6.875
Set 8	6.274
Set 9	6.372
Set 10	6.555
Set 11	6.548

In terms of the quality of the images presented in the Directional Filtering method as can be seen in the images seen in Figures 4.89 and 4.90, noise from the visible spectrum images in Figures 4.1 and 4.2 appears to be amplified in the fused image. However, the visual performance is improved when both images have low levels of noise, and unlike the images from the Greatest Pixel, Wavelet Average, Wavelet Greatest Pixel, and Wavelet Variance Selection methods, contrast within the image is better preserved.

The next method is an adaptation of the Directional Filtering Method. Like all the methods presented thus far, the results of the next method will be compared to the base methods from Section 4.2.

4.6 High-Pass Directional Filtering with Thresholding Results

In the High-Pass Directional Filtering with Threshold method, the best results were produced with a 3×3 window, two levels of wavelet decomposition, and a threshold of 80. The current method is a modification of the Directional Filtering method by averaging the LL band and using a threshold for fusion in the high-

Fig. 4.100.: The result of applying the High-Pass Directional Filtering with Thresholding method to the images in Figure 4.1

Fig. 4.101.: The result of applying the High-Pass Directional Filtering with Thresholding method to the images in Figure 4.2

pass images. Figures 4.100 through 4.110 depict the performance of the High-Pass Directional Filtering with Thresholding method on the images in Figures 4.1 through 4.11.

Fig. 4.102.: The result of applying the High-Pass Directional Filtering with Thresholding method to the images in Figure 4.3

Fig. 4.103.: The result of applying the High-Pass Directional Filtering with Thresholding method to the images in Figure 4.4

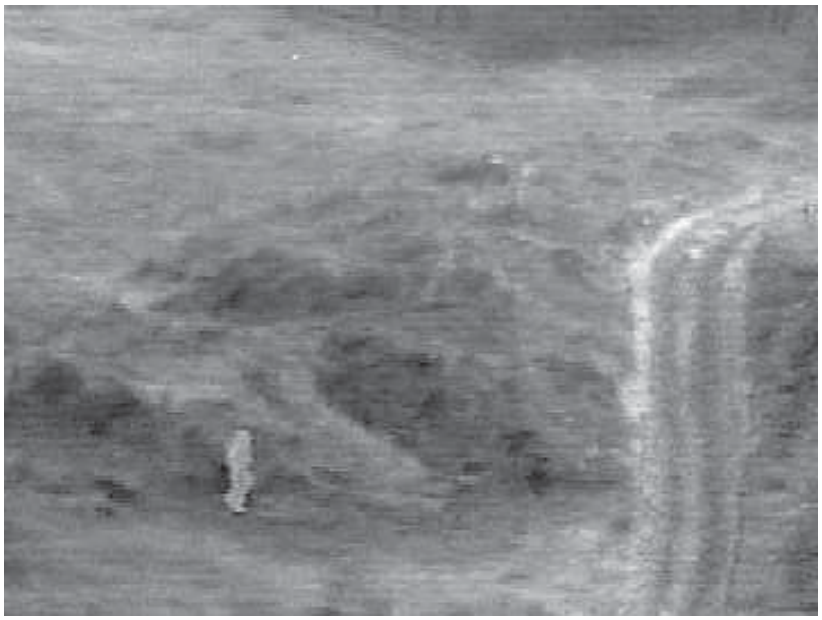

Fig. 4.104.: The result of applying the High-Pass Directional Filtering with Thresholding method to the images in Figure 4.5

Fig. 4.105.: The result of applying the High-Pass Directional Filtering with Thresholding method to the images in Figure 4.6

Fig. 4.106.: The result of applying the High-Pass Directional Filtering with Thresholding method to the images in Figure 4.7

Fig. 4.107.: The result of applying the High-Pass Directional Filtering with Thresholding method to the images in Figure 4.8

Fig. 4.108.: The result of applying the High-Pass Directional Filtering with Thresholding method to the images in Figure 4.9

Fig. 4.109.: The result of applying the High-Pass Directional Filtering with Thresholding method to the images in Figure 4.10

Fig. 4.110.: The result of applying the High-Pass Directional Filtering with Thresholding method to the images in Figure 4.11

From the images it can be seen that the High-Pass Directional Filtering with Thresholding method is consistently out performed by many of the methods presented in Section 4.2. In addition, based on the entropy values of Table 4.5 and Table 4.1, it is apparent that the results are not very strong for the proposed method. It is to be noted that like the high-pass method results from Section 4.4, the performance of the Wavelet Average while better than the High-Pass Directional Filtering with Thresholding method yet both have comparable performance. This is due to the fact that the proposed method uses averaging on the LL band of the image instead of regional variance.

The entropy results obtained from the High-Pass Directional Filtering with Thresholding are again similar to the entropy values obtained from the Wavelet Variance Selection method. In most cases, the entropy values in the High-Pass Directional Filtering method are less than the Wavelet Variance Selection method, but difference between the two methods is relativity small.

While the entropy values for High-Pass Directional Filtering with Thresholding do not suggest that the method performs well, yet from a qualitative standpoint, the method has more consistent performance across noisy and low-noise images. From

Table 4.5: Entropy values of the images displayed in Figure 4.100 through 4.110

Entropy Results	
Set	**High-Pass Directional Filtering with Thresholding**
Set 1	5.867
Set 2	6.490
Set 3	6.130
Set 4	6.320
Set 5	7.055
Set 6	5.409
Set 7	6.698
Set 8	5.649
Set 9	6.334
Set 10	6.236
Set 11	6.260

the images shown in Figures 4.100 and 4.101, its performance is similar to that of the Wavelet Average method seen in Figures 4.45 and 4.46. In addition, the High-Pass Regional Variance method exhibits good performance in Figures 4.107 and 4.108 similar to the results from the Wavelet Greatest Pixel method in Figures 4.41 and 4.42. While the performance of the Wavelet Greatest Pixel, Wavelet Average, and Wavelet Variance Selection methods fluctuate based on the scene, the High-Pass Regional Variance method excels by providing consistent output quality regardless of the scene.

In the next section, the results for the Directional Filtering with an Adaptive Threshold method will be presented. After presenting the results, the method will be compared with the base methods from Section 4.2.

4.7 Directional Filtering with an Adaptive Threshold Results

The final method proposed is that of Directional Filtering with an Adaptive Thresholding. This method uses regional variance with different windows in the

high-pass images, three levels of wavelet decomposition, and a fixed threshold of 70. The performance of this method is shown in Figures 4.111 through 4.121.

Fig. 4.111.: The result of applying the Directional Filtering with an Adaptive Threshold method to the images in Figure 4.1

In terms of entropy, the Directional Filtering with an Adaptive Threshold consistently out performs many of the methods in Section 4.2. Comparing the values of Table 4.6 and Table 4.1, there are a few situations where the Wavelet Average method out performs the proposed method; however, the results are very close. In other cases, the the Wavelet Greatest Pixel method out performs the proposed method. While the proposed method is not the top performer in most cases, it is consistently one of the top performing methods.

For most sets of input images, the entropy values obtained from the Directional Filtering with an Adaptive Threshold method are consistently higher than the entropy values from the Wavelet Variance Selection method. Out of all the proposed methods, the Directional Filtering with an Adaptive Threshold method out performs the Wavelet Regional Variance method more often and with greater differences.

As can be seen, the images in Figures 4.111 through 4.114 are very similar to the images produced in Figures 4.45 through 4.48 respectively. The proposed method's performance is similar to that of the Wavelet Average method; however, in the cases

Fig. 4.112.: The result of applying the Directional Filtering with an Adaptive Threshold method to the images in Figure 4.2

Fig. 4.113.: The result of applying the Directional Filtering with an Adaptive Threshold method to the images in Figure 4.3

Fig. 4.114.: The result of applying the Directional Filtering with an Adaptive Threshold method to the images in Figure 4.4

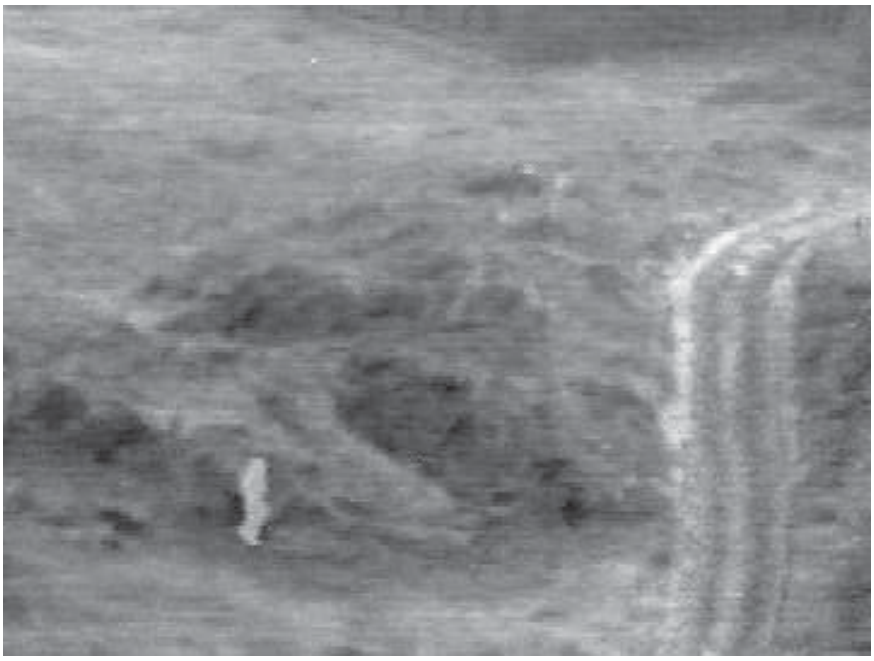

Fig. 4.115.: The result of applying the Directional Filtering with an Adaptive Threshold method to the images in Figure 4.5

Fig. 4.116.: The result of applying the Directional Filtering with an Adaptive Threshold method to the images in Figure 4.6

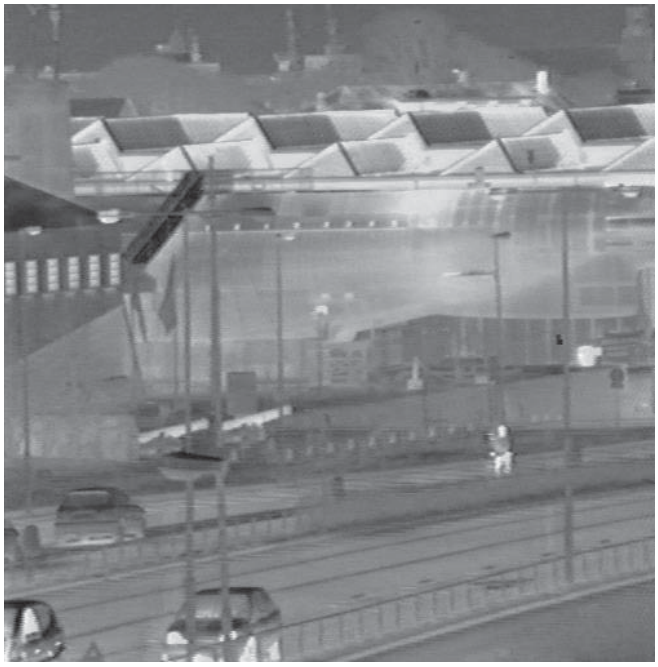

Fig. 4.117.: The result of applying the Directional Filtering with an Adaptive Threshold method to the images in Figure 4.7

Fig. 4.118.: The result of applying the Directional Filtering with an Adaptive Threshold method to the images in Figure 4.8

Fig. 4.119.: The result of applying the Directional Filtering with an Adaptive Threshold method to the images in Figure 4.9

Fig. 4.120.: The result of applying the Directional Filtering with an Adaptive Threshold method to the images in Figure 4.10

Fig. 4.121.: The result of applying the Directional Filtering with an Adaptive Threshold method to the images in Figure 4.11

Table 4.6: Entropy values of the images displayed in Figure 4.111 through 4.121

Entropy Results	
Set	**Directional Filtering with an Adaptive Threshold**
Set 1	5.734
Set 2	6.341
Set 3	6.535
Set 4	6.466
Set 5	7.105
Set 6	5.981
Set 7	7.043
Set 8	6.200
Set 9	6.448
Set 10	6.766
Set 11	6.817

where the Wavelet Average method has poor performance, the Directional Filtering with an Adaptive Threshold method has better performance. Similarly, when comparing the results of the Wavelet Greatest Pixel method in Figures 4.41 and 4.42 to the results of the Directional Filtering with an Adaptive Threshold in Figures 4.118 and 4.119 the performance is comparable. However, where the Wavelet Greatest Pixel Method has poor performance, the visual quality of fusion from the Directional Filtering with an Adaptive Threshold method is maintained.

Now that the results of each of the five proposed methods have been presented, the next section will focus on analyzing each method. Using qualitative analysis, the results will be discussed for all methods presented in Sections 4.3 through 4.7.

4.8 Qualitative Analysis

Overall, the methods presented in the Section 4.3 through 4.7 were often consistent across the various images presented in Figures 4.1 through 4.11. In order to have a good image fusion algorithm, the method must be able to work in a variety

of situations, not just extreme ones. Throughout the remainder of this section, a comparison of the five methods will be made.

In many cases, the results of the High-Pass Regional Variance and High-Pass Directional Filtering with Thresholding methods look very similar to that of the Wavelet Average method. In addition since the LL bands within these methods are averaged together, in some cases, especially in the fusion of the images in Figure 4.6, much of the infrared data is diminished. Instead of enhancing the image in the regions with high infrared activity, the tendency of these images is to reduce the brightness.

The Regional Variance method and Directional Filtering methods are two methods that seem to handle images with strong infrared or visible information better than the the High-Pass Regional Variance and High-Pass Directional Filtering with Thresholding methods. In Figures 4.72 and 4.94, each method accentuates the regions with high infrared from Set 6 in Figure 4.6 activity much better than the high-pass methods represented in Figures 4.83 and 4.105. Even though the Regional Variance and Directional Filtering methods help when regions have more content in one image over the other, these two methods have poor performance in high noise situations. The the High-Pass Regional Variance and High-Pass Directional Filtering with Thresholding methods had better performance in noisy images, specifically the images from Figures 4.1 and 4.2.

The last method, the Directional Filtering with an Adaptive Threshold method, is a method that has the best overall performance working with noisy images while accentuating content well in both input images. While the high amount of content in Figure 4.116 does not accentuate the infrared image as in Figures 4.72 and 4.94, there is a good compromise in the performance. Particularly, when fusing noisy images, the Directional Filtering with an Adaptive Threshold method does not accentuate noise the way that the Regional Variance or Directional Filtering methods will.

In conclusion, the results indicate that there are three methods that perform better than the other image fusion methods. In the case of noisy images, the Directional Filtering with an Adaptive Threshold has the most consistency over the other methods.

On the other hand, when noise is not an issue, the Regional Variance and Directional Filtering methods perform well.

5. CONCLUSIONS AND FUTURE WORK

Throughout this thesis, five new multiresolution image fusion methods have been proposed. In addition to using wavelet transforms, the proposed methods use local variance estimates to obtain fusion weights.

The Regional Variance, High-Pass Regional Variance, Directional Filtering, High-Pass Directional Filtering with Thresholding, and Directional Filtering with an Adaptive Threshold methods were proposed throughout this thesis. Using entropy to measure performance, the proposed methods were compared against some common methods including the Pixel Average, Greatest Pixel Value, Wavelet Average, Wavelet Greatest Pixel, and Wavelet Variance Selection methods.

The results of each proposed method were more consistent than the base methods. Results indicate that the High-Pass Regional Variance and High-Pass Directional Filtering with Thresholding methods had difficulties performing better than the Wavelet Average method because the LL bands of the two proposed methods relied on averaging. The Regional Variance and Directional Filtering methods outperformed the High-Pass Regional Variance and High-Pass Directional Filtering with Thresholding methods by performing fusion without reducing the overall contrast of the output image. While these methods did perform well in most cases, noise in either input image was amplified in the output. This lead to the final proposed method: Directional Filtering with an Adaptive Threshold. This method did not have the same performance as the Regional Variance and Directional Filtering methods; however, the results were considerably better than the High-Pass Regional Variance and High-Pass Directional Filtering with Thresholding methods, and noise was not amplified throughout the fusion process.

From the issues that arose with proposed methods, there are few areas of research for future development of image fusion techniques. In the case of the Regional Vari-

ance and Directional Filtering methods, modifications to the preprocessing stage or within the fusion step itself may assist with noise suppression.

Entropy values of the base methods and proposed methods are rather close, and the variance of entropy values of the proposed methods is small. In order to further determine the effectiveness of the proposed methods, a statistical analysis using hypothesis testing is needed.

Further work can be carried out to Directional Filtering. As stated before, the issue with the High-Pass Regional Variance and High-Pass Directional Filtering with Thresholding methods is the fact that the results are similar to the Wavelet Average method. In order to enhance image fusion techniques that use wavelet transforms, it is recommended to use information in the high-pass images to fuse the LL images. For example, if variance in the HH image is stronger than the variance in the LH and HL images, use a diagonal window to fuse the region in the LL image. Investigating this technique may provide new avenues for image fusion in the wavelet domain.

LIST OF REFERENCES

LIST OF REFERENCES

[1] Z. Wang, D. Ziou, C. Armenakis, D. Li, and Q. Li, "A comparative analysis of image fusion methods," *IEEE Transactions on Geoscience and Remote Sensing*, vol. 43, pp. 1391–1402, June 2005.

[2] Z. Guo and J. Yang, "Wavelet transform image fusion based on regional variance," *SPIE*, vol. 6790, 2009.

[3] S. Rahman, M. Ahmad, and M. Swamy, "Contrast-based fusion of noisy images using discrete wavelet transform," *IET Image Processing*, vol. 4, pp. 374 –384, Oct. 2010.

[4] J. Kern and M. Pattichis, "Robust multispectral image registration using mutual-information models," *IEEE Transactions on Geoscience and Remote Sensing*, vol. 45, pp. 1494 –1505, May 2007.

[5] A. Ellmauthaler, C. Pagliari, and E. da Silva, "Multiscale image fusion using the undecimated wavelet transform with spectral factorization and nonorthogonal filter banks," *IEEE Transactions on Image Processing*, vol. 22, pp. 1005–1017, March 2013.

[6] T. Sahoo, S. Mohanty, and S. Sahu, "Multi-focus image fusion using variance based spatial domain and wavelet transform," *2011 International Conference on Multimedia, Signal Processing, and Communication Technologies (IMPACT)*, pp. 48–51, Dec. 2011.

[7] A.-C. Wang and P. Zhao, "Multi-focus image fusion with the double-density dual-tree dwt," *2008 Congress on Image and Signal Processing*, vol. 4, pp. 371–374, May 2008.

[8] H. hui Wang, J.-X. Peng, and W. Wu, "A fusion algorithm of remote sensing image based on discrete wavelet packet," *2003 International Conference on Machine Learning and Cybernetics*, vol. 4, pp. 2557 – 2562 Vol.4, Nov. 2003.

[9] R. Huan and Y. Pan, "Decision fusion strategies for sar image target recognition," *IET Radar, Sonar Navigation*, vol. 5, pp. 747–755, Aug. 2010.

[10] B. Luo, M. Khan, T. Bienvenu, J. Chanussot, and L. Zhang, "Decision-based fusion for pansharpening of remote sensing images," *IEEE Geoscience and Remote Sensing Letters*, vol. 10, pp. 19–23, Jan. 2013.

[11] H. Yang, Q. Du, and B. Ma, "Decision fusion on supervised and unsupervised classifiers for hyperspectral imagery," *IEEE Geoscience and Remote Sensing Letters*, vol. 7, pp. 875–879, Oct. 2010.

[12] A. Siddiqui, M. Jaffar, A. Hussain, and A. Mirza, "Block-based feature-level multi-focus image fusion," *2010 5th International Conference on Future Information Technology (FutureTech)*, pp. 1–7, May 2010.

[13] N. Yu, T. Qiu, F. Bi, and A. Wang, "Image features extraction and fusion based on joint sparse representation," *IEEE Journal of Selected Topics in Signal Processing*, vol. 5, pp. 1074–1082, Sept. 2011.

[14] T. Wan, N. Canagarajah, and A. Achim, "Segmentation-driven image fusion based on alpha-stable modeling of wavelet coefficients," *IEEE Transactions on Multimedia*, vol. 11, pp. 624–633, June 2010.

[15] T. Wan, N. Canagarajah, and A. Achim, "Multiscale color-texture image segmentation with adaptive region merging," *2007 IEEE International Conference on Acoustics, Speech and Signal Processing (ICASSP 2007)*, vol. 1, pp. I–1213–I–1216, April 2007.

[16] T. Wan, N. Canagarajah, and A. Achim, "Statistical multiscale image segmentation via alpha-stable modeling," *2007 IEEE International Conference on Image Processing (ICIP 2007)*, vol. 4, pp. IV – 357–IV – 360, Oct. 2007.

[17] S. Chen, R. Zhang, H. Su, J. Tian, and J. Xia, "Sar and multispectral image fusion using generalized ihs transform based on á trous wavelet and emd decompositions," *IEEE Sensors Journal*, vol. 10, no. 3, pp. 737–745, 2010.

[18] M. Choi, "A new intensity-hue-saturation fusion approach to image fusion with a tradeoff parameter," *IEEE Transactions on Geoscience and Remote Sensing*, vol. 44, pp. 1672–1682, June 2006.

[19] H. Chu and W. Zhu, "Fusion of ikonos satellite imagery using ihs transform and local variation," *IEEE Geoscience and Remote Sensing Letters*, vol. 5, pp. 653–657, Oct. 2008.

[20] M. Chikr El-Mezouar, N. Taleb, K. Kpalma, and J. Ronsin, "An ihs-based fusion for color distortion reduction and vegetation enhancement in ikonos imagery," *IEEE Transactions on Geoscience and Remote Sensing*, vol. 49, pp. 1590–1602, May 2011.

[21] X. Zhang, "Infrared and color visible image sequence fusion based on statistical model and image enhancement," *2008 International Conference on Advanced Computer Theory and Engineering (ICACTE 2008)*, pp. 934–937, Dec. 2008.

[22] L. Chun-Lin, *A Tutorial of the Wavelet Transform.* Walden University, Feb. 2010.

[23] J. Nunez, X. Otazu, O. Fors, A. Prades, V. Pala, and R. Arbiol, "Multiresolution-based image fusion with additive wavelet decomposition," *IEEE Transactions on Geoscience and Remote Sensing*, vol. 37, pp. 1204–1211, May 1999.

[24] H. Wu and Y. Xing, "Pixel-based image fusion using wavelet transform for spot and etm+ image," *2010 IEEE International Conference on Progress in Informatics and Computing (PIC)*, vol. 2, pp. 936–940, Dec. 2010.

[25] Y. Guo, M. Xie, and L. Yang, "An adaptive image fusion method based on local statistical feature of wavelet coefficients," *2009 International Symposium on Computer Network and Multimedia Technology (CNMT 2009)*, pp. 1–4, Jan. 2009.

[26] H. Tian, Y.-N. Fu, and P.-G. Wang, "Image fusion algorithm based on regional variance and multi-wavelet bases," *2010 2nd International Conference on Future Computer and Communication (ICFCC)*, vol. 2, pp. V2–792–V2–795, May 2010.

[27] Y.-H. Tsai and Y.-H. Lee, "Wavelet-based image fusion by adaptive decomposition," *2008 Eighth International Conference on Intelligent Systems Design and Applications (ISDA 2008)*, vol. 2, pp. 283–287, Nov. 2008.

[28] U. Patil and U. Mudengudi, "Image fusion using hierarchical pca.," *2011 International Conference on Image Information Processing (ICIIP)*, pp. 1–6, Nov. 2011.

[29] Z. Guang, Z. Zhao, Q. Gao, and S. Wang, "Infrared and visible images fusion based on contourlet-domain hidden markov tree model," *2011 4th International Congress on Image and Signal Processing (CISP)*, vol. 4, pp. 1916–1920, Oct. 2011.

[30] A. Mumtaz and A. Majid, "Genetic algorithms and its application to image fusion," *2008 4th International Conference on Emerging Technologies (ICET 2008)*, pp. 6–10, Oct. 2008.

[31] J. Toontham, W. Rattanapitak, and S. Udomhunsakul, "Comparative efficiency of wavelet filters for multi-focus color image fusion," *2010 2nd International Conference on Education Technology and Computer (ICETC)*, vol. 5, pp. V5–87 –V5–91, June 2010.

[32] J. Lewis, S. Nikolov, C. Canagarajah, D. Bull, and A. Toet, "Uni-modal versus joint segmentation for region-based image fusion," *2006 9th International Conference on Information Fusion*, pp. 1–8, July 2006.